A multimessenger story: Using electromagnetic and gravitational wave detections of binary black holes to improve parameter estimation

Author: Joan Llobera Querol

Supervisor: Dr. Tamara Bogdanović

Co-supervisor: Dr. Deirdre Shoemaker

Tutor: Dr. Ramon Torres

Bachelor's Thesis

Grau en Matemàtiques - Grau en Enginyeria Física

May 2020

Abstract: A coalescence of two supermassive black holes (SMBHs) is expected to produce copious amounts of gravitational waves (GWs) and in general, a remnant SMBH that is recoiling with respect to the center of mass of its parent binary. When the SMBH coalescence occurs in a gas-rich galaxy, GWs may be accompanied by a luminous electromagnetic (EM) counterpart. Systems of SMBHs for which both emission signatures can be detected will provide us with a unique opportunity to decode the properties of the pre-merger binaries from GWs and to determine the speed of the recoiling remnant from EM observations. There is a consensus among astrophysicists that combined together, the GW and EM detections should provide stronger constraints on the properties of merging binaries than either one in isolation, but the quantitative implications of such detections are yet to be understood. Motivated by this question, we investigate the improvement in SMBH binary parameter estimation brought about by the multimessenger detections of their mergers and quantify which binary configurations will benefit the most from this approach. The results of this work are of direct importance for the future space-based GW observatory LISA and are also relevant to all other GW and EM observatories that will partake in multimessenger detections of coalescing black hole binaries.

keywords: black hole, general relativity, astrophysics, black hole binaries, merger, gravitational waves, multimessenger, parameter estimation.

AMS classification code (MSC2010): 83C57

Resum: Es creu que la fusió de dos forats negres supermassius produeix una gran intensitat d'ones gravitacionals i, en general, un forat negre resultant que retrocedeix respecte al centre de masses del sistema binari predecessor. Si la coalescència es produeix en una galàxia rica en gas, es pot observar també una contrapartida electromagnètica força lluminosa. Els sistemes de forats negres supermassius en què es puguin detectar ambdues emissions ens oferiran una oportunitat única per descodificar les propietats dels forats negres originals a partir de les ones gravitacionals i també determinar la velocitat del forat negre resultant a partir de les observacions electromagnètiques. El consens entre astrofísics és que les dues emissions combinades podrien establir restriccions més fortes a les propietats dels forats negres en procés de fusió que una sola emissió, tanmateix encara no es coneixen les implicacions quantitatives d'aquestes deteccions múltiples. Motivats per aquesta qüestió, investiguem la millora en l'estimació de paràmetres en sistemes binaris de forats negres supermassius que suposarien les esmentades deteccions múltiples i quantifiquem quines configuracions se'n veurien més beneficiades. Els resultats d'aquest treball són d'importància directa per al futur observatori d'ones gravitacionals LISA i també són rellevants per a tots els altres observatoris d'ones gravitacionals i electromagnètiques que poden formar part de deteccions múltiples de fusions de forats negres supermassius.

paraules clau: forat negre, relativitat general, astrofísica, sistemes binaris de forats negres, fusió, ones gravitacionals, detecció múltiple, estimació de paràmetres.

This project would not have been possible without the support and collaboration of many. I would like to thank specially CFIS and Fundació Privada Cellex, for granting me the opportunity of doing my Bachelor's Thesis abroad and their financial support.

I would also like to thank Dr. Tamara Bogdanović, for her guidance, her kindness, and her approachability and Dr. Deirdre Shoemaker, for her support and her closeness. I am very grateful for their generous advice throughout my stay at GeorgiaTech and for letting me be a part of their groups at the CRA. I would like to thank as well Dr. Ramon Torres, for accepting being my tutor at UPC and his long-distance accompaniment.

I would like to thank specially Adrià, my great companion these past months. I would also like to mention all the people that I met at GeorgiaTech, for making my stay fuller in their own way, to prof. Laguna, Khai, Miguel, Deborah, Matt, Simon, Sudarshan, Lily, Yupeng and everyone at the CRA; to Scott, the OIE staff, Clément, Gabriel and the other international colleagues; to the amazing people from Chorale, and to my new Pi Ep family, which I will always be proud to be a part of.

To everyone that has encouraged me and prepared me in my scientific career, specially to my high school teachers and the organizers of the activities I have participated in during my teen years (Olympiads, Cangur, Joves i Ciència...). To my peers at CFIS, for all the discussions and the good moments throughout these years.

I a la meva família, i a tots aquells que us heu interessat pel que feia malgrat no entendre-ho massa. Gràcies per ser-hi.

We were born of stars and in death we will return to them.
Let's not strive to be black holes in the meantime.

Courtney M. Privett (Arrow of Entropy)

Contents

List of Figures

List of Tables

Chapter 1

Preamble

Black holes are some of the most interesting and mysterious objects of the universe. Nearly everyone has heard of them and is fascinated with their seemingly unstoppable hunger and ability to swallow anything that gets too close.

The reality is that black holes are a prediction of Albert Einstein's Theory of General Relativity that has been verified throughout the 20th century and continues to be tested in this century. At present time many astrophysicists around the globe work on observations, characterization, modeling, and processes involving black holes, but the mystery around them is only starting to get untangled.

Supermassive black holes experience mergers that are among the most energetic processes in the universe. These events produce different signatures that are observable from Earth, as gravitational and electromagnetic waves. Observation of these signals is the key for parameter estimation and deciphering the properties of the emitting systems.

In this thesis, we assess the benefits of the multimessenger approach for parameter estimation in binary black holes. We use measurements of the recoil velocity of the remnant black hole to improve parameter estimation and provide one of the first quantitative estimates of performance of this approach for supermassive black hole mergers.

The rest of this thesis is organized as follows: in section 2 we provide the observational and theoretical background, in section 3 we describe the algorithm for analysis of the gravitational wave recoil, provide results in section 4, discuss implications of our findings for observations in section 5 and conclude in section 6.

Chapter 2

Introduction

2.1 Observational evidence for recoiling MBHs

Galaxy mergers are an important process for galaxy growth and formation of large-scale structure in the universe. Observations show that nearly all massive galaxies at low redshift contain a supermassive black holes (SMBHs) at their center. Evolution of such SMBHs and their host galaxies are strongly connected (Ferrarese & Merritt, 2000) and it has been predicted for a while that when galaxies merge, so do their central black holes (Begelman et al., 1980).

When the SMBHs are separated by galactic distances (on the order of kpc), gravitational wave (GW) emission alone is too weak to cause the merger in less than a Hubble time (Pretorius, 2007, and references therein). At these separations, dynamical friction is the main process involved in the dissipation of the SMBHs' orbital energy (Boylan-Kolchin et al., 2008). The pairs of SMBHs that continue to sink to separations of a few pc will have a chance to form a gravitationally bound system. Due to gravitational slingshot and ejection of stars and gas by the SMBH binary, matter can become partially depleted in vicinity of its orbital path. Some models show that this could substantially slow down the binding process of SMBHs at separations of $\sim 1\,\mathrm{pc}$, effectively causing them to stall and never experience a merger. Multiple methods have been proposed to solve this stalling, like the loss-cone refilling by gradual scattering of stars into the SMBH binary path (Milosavljević & Merritt, 2003), or via dynamical interactions of multiple BHs (Ryu et al., 2018), while some suggest that this problem can be resolved by relying on less idealized models of merger remnant galaxies (Berczik et al., 2006).

SMBH binaries that reach the milliparsec scales find themselves in the inspiral

regime dominated by GW emission and coalesce, giving birth to a daughter black hole (Hawking, 1972), with a powerful emission of GWs, accompanied potentially by EM waves. Emitted GWs carry away energy and linear momentum but are not symmetric in all spatial directions. Namely, strong emission that occurs in the last few orbits before BH coalescence is asymmetric in general case. As a consequence of conservation of linear momentum the daughter black hole recoils in the opposite direction (Bekenstein, 1973).

Recoiling SMBHs are challenging to unambiguously identify in observations. Even though the frequency of Active Galatic Nuclei (AGNs) hosting SMBH binaries is certainly low (Bogdanović, 2015), research shows that AGN surveys like the Sloan Digital Sky Survey (SDSS)[1] may contain hundreds of spatially offset AGNs, and therefore motivate a careful search for recoiling AGNs within those archives (Blecha et al., 2016). Many methods have been suggested to search for such SMBHs. Accretion from interstellar medium produces too low luminosity for a SMBH to be observed but the recoiling SMBH is expected to carry a fraction of the accretion disk with it, allowing it to shine while accreting mass for $\sim 10^7$ yrs (Loeb, 2007). Therefore, one would expect a recoiling SMBH to be spatially offset from the center of its galaxy and/or to have a non-zero velocity offset with respect to the rest frame of the galaxy, that can in principle be detected in spectroscopic searches (Bogdanović, 2015).

Numerous candidates for recoiling SMBHs have been found (Komossa, 2012; Blecha et al., 2019). Some searches look for offset in the velocity frame by identifying Doppler-shifted broad emission lines in the optical spectra of AGNs. For example, Bonning et al. (2007) analyze SDSS quasars with measurable velocity offsets but are cautious in claiming that these are recoiling SMBHs. Komossa et al. (2008) identify a compeling candidate for recoiling SMBH with velocity offset of $\sim 2650\ \mathrm{km\,s^{-1}}$ but again show no decisive evidence. Bogdanović et al. (2009) and Dotti et al. (2009) argued that this source could also be explained as a binary black hole (BBH) system in which the only the secondary BH is active and Vivek et al. (2009) suggest some additional explanation. Robinson et al. (2010) present another quasar as a binary black hole candidate and point out that outflowing wind carrying the broad-line emission can be alternative explanation. Eracleous et al. (2012) carry out a systematic search using the SDSS quasars to conclude that the most promising candidates could be described both as recoiling BHs or SMBH binaries. More recently, Kim et al. (2017) perform a systematic search within the Chandra X-ray

[1] `https://www.sdss.org/`

observatory[2] and SDSS catalogs and identify a quasar consistent both the recoiling SMBH and the dual SMBH scenarios. Chiaberge et al. (2018) show a quasar with observations supporting the recoiling BH scenario but with no conclusive proof. Finally, Kim et al. (2018) detect temporal patterns on the velocity offset of a quasar and suggest the scenario of an oscillating recoiling SMBH.

Other searches have looked for spatial offsets. Jonker et al. (2010) present an unusual X-ray source located 3.2 kpc from the nucleus of the host galaxy, exploring three scenarios: a very bright supernova, an off-nuclear ultraluminous X-ray source powered by an intermediate mass black hole in a star cluster, or a recoiling SMBH. For another source, Koss et al. (2014) discuss an emission consistent with an outburst from a luminous blue variable star, an infalling dwarf galaxy or a recoiling black hole, for which Stanek et al. (2019) inform of a recent rebrightening. Markakis et al. (2015) describe an object consistent with a BBH or a SMBH recoiling at $v \sim 355$ km s^{-1}, although not evidence unambiguously supports that scenario. Finally, Kalfountzou et al. (2017) present a galactic triplet with three possible interpretations: a SMBH triplet with two active BHs, a triple-AGN merger with a poorly-active third nucleus, or an ejected SMBH due to a slingshot through the interaction with the other two BHs.

Our interest goes beyond merely a detection of recoiling SMBH and it includes measuring their recoil velocity. Observations of Doppler-shifted optical broad emission lines are a direct method to obtain the radial velocity, v_r (i.e. component projected onto the line of sight). Imaging of a spatial offset on the other hand can place constraints on the component of the recoil velocity in the plane of the sky and equivalently, the time since the BH has been kicked. Coincidental detections of both spatial and velocity offset from the same source are however uncommon: one really promising example is CID-42, first described in Civano et al. (2010) as two optical sources 2.5 kpc away from each other with a X-ray source that could be either going through the first close passage in a galactic merger or a post-merger recoiling BH. Further studies (Civano et al., 2012; Blecha et al., 2013; Chiaberge et al., 2017) do not allow either scenario to be ruled out. These observational efforts illustrate how challenging it is to unambiguously identify recoiling BHs with EM observations alone.

Fortunately, SMBH mergers are also a powerful source of GWs, so joint detection of an EM counterpart would make things much easier. A GWs detection in the

[2] `https://cxc.harvard.edu/index.html`

low frequency range ($f \lesssim 10^{-3}$ Hz) would be a compelling indicator of a SMBH merger (Hawking & Israel, 1979). Detections of this type are considered one of the prime scientific goals for the future space-based GW observatory LISA (Laser Interferometer Space Antenna[3]), which will be launched in the mid-2030s. LISA will permanently scan the sky in the search for GWs with frequencies matching those emitted during the SMBH inspiral and coalescence (Amaro-Seoane et al., 2017). If simultaneously with or after a GW detection EM searches can pinpoint the location of the merger on the sky, astronomers would be able to rule out most alternative scenarios to a recoiling AGN.

SMBH binaries are not the only kind that after coalescence may give rise to recoiling remnant BHs. Stellar origin black holes, produced in gravitational collapse of massive stars, can also exist in binaries and experience coalescence. Indeed, mergers of stellar origin BHs have been detected many times over the past 4 years by the LIGO-Virgo observatory (Abbott et al., 2016, 2019). Stellar origin BHs are however thought to live in gas-poor environments in majority of cases. If so, such BHs will not be active and their GW signal may lack an EM counterpart. This is the reason why this thesis focuses on SMBH binaries, even though many of the findings presented here are in principle applicable to both populations of BHs.

2.2 Theoretical background

When GW recoil was first predicted by relativists more than 50 years ago (Peres, 1962; Bekenstein, 1973), it was expected to be considerably smaller than 1500 $\mathrm{km\,s^{-1}}$ (Fitchett, 1983) and of no significant consequence for SMBH dynamics. Since most of the kick is “accumulated" in the strongly non-linear regime of BBH evolution near the coalescence, numerical relativity (NR) simulations, capable of solving the Einstein equations of general relativity on dynamic spacetimes (created by orbiting BHs), are the only approach that can predict recoil speeds from the first principles. First NR simulations of BBH mergers brought to light the actual power of the recoil just 15 years ago (Brügmann et al., 2004; Pretorius, 2005; Campanelli et al., 2006a,b). The first studies of GW kicks tried to replicate theoretical expectations from (Fitchett & Detweiler, 1984), showing that mergers of non-spinning binaries could lead to kicks up to ~ 175 $\mathrm{km\,s^{-1}}$ (Baker et al., 2006; Herrmann et al., 2007a; González et al., 2007b). Subsequent studies of BHs of equal masses with aligned and antialigned spins resulted in kicks as high as 475 $\mathrm{km\,s^{-1}}$ (Herrmann et al.,

[3]https://www.elisascience.org

2007b; Koppitz et al., 2007; Pollney et al., 2007), with more generic configurations achieving 2500 $\mathrm{km\,s^{-1}}$ (González et al., 2007a). Following studies suggested that GW recoil velocities could be as high as $\sim$ 4000 $\mathrm{km\,s^{-1}}$ in the so called "super-kick" configuration, involving an equal-mass binary with the spin vectors of equal magnitude, lying in the orbital plane and with direction opposite to one another (Campanelli et al., 2007a,b; Brügmann et al., 2008). A few years later, another configuration, the "hang-up" kick was found to be able to generate a kick of up to 5000 $\mathrm{km\,s^{-1}}$ (Lousto & Zlochower, 2011a). These kick velocities are obtained for the case of BH binaries on quasi-circular orbits, thought to be of astrophysical relevance. Healy et al. (2009) nevertheless showed that high-eccentricity encounters could in principle generate even larger kick velocities, of the order of $10,000$ $\mathrm{km\,s^{-1}}$.

These discoveries triggered substantial interest among astronomers, because a remnant SMBH with such large recoil velocity would be able to escape the nucleus of even the most massive host galaxy (Merritt et al., 2004). Therefore, one might expect that many galaxies that have experienced a merger would not have a SMBH in its center. Observations however show that it is not the case, since almost all major galaxies seem to have the central SMBHs (Richstone et al., 1998). Some works, like Schnittman (2007), point out that even with large escape velocities, the fraction of observed galaxies with SMBHs should be high; and theoretical studies like Bogdanović et al. (2007) show that mergers in gas-rich environments lead to spin alignment with the orbital angular momentum and low kick velocities. Following that logic, one may expect to find remnant BHs with lower kick velocities in gas-rich environments, such as mergers of gas-rich galaxies.

Motivated by these findings, both relativists and astronomers became interested in modeling the kick dependence on the binary parameters and finding compelling candidates for recoiling SMBHs in observations. First simulations suggested that kick velocity depends strongly on BH masses and spin configuration. Since GWs also depend on the parameters of the binary (masses and spins of the BHs), one can perform parameter estimation by comparing detected gravitational waveforms with those calculated from NR simulations (Flanagan & Hughes, 1998a,b). These depend on the BH binary parameters in a different way from the GW recoil velocity, so a measurement of both properties would provide independent ways for parameter estimation. Therefore, joint detections of both GWs and GW kick from EM observations would complement each other and could lead to improved measurements of the binary properties.

The goal of this thesis is to explore scenarios when both GW and EM signals

associated with a BH merger can be detected. We evaluate under what conditions will the coincident detections of both messengers result in better constraints of the binary properties relative to the cases where only one such measurement can be made.

2.3 Modeling of the GW recoil velocity

Understanding of the GW kick dependence on the BH binary properties was gradually developed with the advancement of the NR simulations of mergers. Since NR simulations are computationally expensive, it is impractical to carry them out every time one wishes to compute the kick velocity for some binary configuration. As a result, analytic models for the GW kick were developed as a substitute for NR simulations. Because these models are calibrated on a finite but growing set of NR simulations, new generations of models supersede the older ones as new NR simulations come online. For example, Baker et al. (2007) presented first attempts to model the GW kicks from non-precessing binaries and Campanelli et al. (2007a) did it for more generic configurations including precessing binaries. Subsequently, Lousto & Zlochower (2008) and Baker et al. (2008) used more NR simulations to produce analytic fits for the recoil velocity as a function of the BBH parameters.

The models are commonly formulated in terms of the several key parameters, including the total BBH mass $M = m_1 + m_2$, mass ratio $q = m_2/m_1 \leq 1$, relative mass difference $\delta m = \frac{m_1 - m_2}{m_1 + m_2} \geq 0$, and symmetric mass ratio $\eta = \frac{m_1 m_2}{M^2}$. We also define the following dimensionless parameters related to the spin, $\vec{S}$

$$\widetilde{S} = \frac{\vec{S}}{M^2} = \frac{\vec{S}_1 + \vec{S}_2}{M^2} = \frac{\vec{\alpha}_1 + q^2 \vec{\alpha}_2}{(1+q)^2} \tag{2.1}$$

$$\widetilde{\Delta} = \frac{\vec{\Delta}}{M^2} = \frac{\vec{S}_1/m_1 + \vec{S}_2/m_2}{M} = \frac{\vec{\alpha}_1 - q\vec{\alpha}_2}{1+q} \tag{2.2}$$

$$\widetilde{S}_0 = \widetilde{S} - (\delta m/2)\ \widetilde{\Delta} = \frac{\vec{\alpha}_1 + q\vec{\alpha}_2}{1+q} \tag{2.3}$$

where $\vec{\alpha}_i = (c\,\vec{S}_i)/(G\,{m_i}^2)$ is the dimensionless spin vector, $a_i = |\vec{\alpha}_i|$ and index $i = 1, 2$ refers to the primary or secondary black hole. All of these vectors are commonly decomposed to components parallel ($\widetilde{A}_{\parallel} = \widetilde{A} \cdot \hat{L}$) and perpendicular ($\widetilde{A}_{\perp} = \|\widetilde{A} \times \hat{L}\|$) to the orbital angular momentum of the binary.

The models rely on a decomposition first proposed in Campanelli et al. (2007a)

that is still used today

$$\vec{v}_{\rm kick} = v_m\ \hat{e}_1 + v_\perp\left(\cos\xi\ \hat{e}_1 + \sin\xi\ \hat{e}_2\right) + v_\parallel\ \hat{L}, \tag{2.4}$$

where $\parallel$ and $\perp$ are measured with respect to the orbital angular momentum, $\vec{L}$, and $\hat{e}_1, \hat{e}_2$ are the orthogonal unit vectors in the orbital plane. ξ is the angle between the v_m and $v_\perp$ components of velocity.

v_m is the component of the kick velocity contributed by the asymmetry in mass of the BBH system and it depends solely on the mass ratio. First modeled in Campanelli et al. (2007a), it represents the total kick for non-spinning binaries. More recently, this expression for v_m was updated by Healy et al. (2017) who added a fourth-order correction term to it

$$v_m = \eta^2\delta m\left(A + B\delta m^2 + C\delta m^4\right) \tag{2.5}$$

where $A = 8712\ {\rm km\,s^{-1}}$, $B = 6516\ {\rm km\,s^{-1}}$, $C = -3907\ {\rm km\,s^{-1}}$ are the parameters (Healy & Lousto, 2018). We adopt this expression in our modeling described hereafter.

$v_\perp$ is the perpendicular component of kick velocity, which is mostly dependent on the parallel components of the spins (Campanelli et al., 2007a; Baker et al., 2008). It represents the kicks that arise from BBH configurations with aligned spin configurations. This model was subsequently revised several times (Lousto & Zlochower, 2009; Lousto et al., 2010b, 2012; Lousto & Zlochower, 2013). The formulation used in this work was presented in Healy et al. (2014):

$$\begin{aligned} v_\perp = H\eta^2\ \Big(\ & \widetilde{\Delta}_\parallel + H_{2a}\widetilde{S}_\parallel\delta m + H_{2b}\widetilde{\Delta}_\parallel\widetilde{S}_\parallel + H_{3a}\widetilde{\Delta}_\parallel^2\delta m + H_{3b}\widetilde{S}_\parallel^2\delta m + H_{3c}\widetilde{\Delta}_\parallel\widetilde{S}_\parallel^2 \\ & + H_{3d}\widetilde{\Delta}_\parallel^3 + H_{3e}\widetilde{\Delta}_\parallel\delta m^2 + H_{4a}\widetilde{S}_\parallel\widetilde{\Delta}_\parallel^2\delta m + H_{4b}\widetilde{S}_\parallel^3\delta m \\ & + H_{4c}\widetilde{S}_\parallel\delta m^3 + H_{4d}\widetilde{\Delta}_\parallel\widetilde{S}_\parallel\delta m^2 + H_{4e}\widetilde{\Delta}_\parallel\widetilde{S}_\parallel^3 + H_{4f}\widetilde{S}_\parallel\widetilde{\Delta}_\parallel^3\ \Big). \end{aligned} \tag{2.6}$$

We combine it with the parameter values from Healy & Lousto (2018), which are listed in Table 2.1.

$v_\parallel$ is the component of the kick velocity that arises in all configurations in which at least one of the spins is not aligned with the orbital angular momentum. This component is responsible for the high velocity kicks in excess of 500 ${\rm km\,s^{-1}}$ (González et al., 2007a; Campanelli et al., 2007a; Lousto & Zlochower, 2009; Lousto et al., 2010b). Lousto & Zlochower (2011a,b) presented the formula with third-order correction term for equal-mass binaries and Lousto et al. (2012) extended the model

H	7499.115 ± 9.244136	H_{3e}	-0.920198 ± 0.059910
H_{2a}	1.736510 ± 0.032585	H_{4a}	0.434318 ± 0.131104
H_{2b}	-0.598144 ± 0.014548	H_{4b}	1.716134 ± 0.363024
H_{3a}	0.318117 ± 0.032373	H_{4c}	-0.619181 ± 0.249907
H_{3b}	0.748613 ± 0.115497	H_{4d}	1.633127 ± 0.195661
H_{3c}	-1.749784 ± 0.028088	H_{4e}	-2.253606 ± 0.236644
H_{3d}	-0.011247 ± 0.002264	H_{4f}	-0.028194 ± 0.041426

Table 2.1: Fitting parameters (in $\mathrm{km\,s^{-1}}$) for equation (2.6), as provided in Healy & Lousto (2018)

to generic mass ratios. A major breakthrough in modeling was achieved with implementation of the hangup kick in the model (Lousto & Zlochower, 2013). Hangup configuration is an equal-mass binary with maximal spins, oriented at 50° with respect to the orbital angular momentum and pointing in the directions opposite to each other. This configuration produces a kick of nearly 5000 $\mathrm{km\,s^{-1}}$, the highest velocity predicted for quasi-circular mergers. This question was examined in more detail in Zlochower & Lousto (2015), that presents the state of the art model for this component, used in this work.

$$v_{\parallel} = V_1 \cos\Phi_0 \tag{2.7}$$

$$V_1 = \sqrt{V_{\rm h}^2 + V_{\rm c}^2 + 2V_{\rm h}V_{\rm c}\cos\left(59\pi/180\right)} \tag{2.8}$$

$$V_{\rm h} = (4\eta)^2 \widetilde{\Delta}_{\perp}\left[D\left(\frac{1 + c_1\delta m^2 + E\widetilde{S}_{0\parallel}}{1 + F\widetilde{S}_{0\parallel}}\right) + c_9\delta m\widetilde{\Delta}_{\parallel}\right] \tag{2.9}$$

$$V_{\rm c} = (4\eta)^2 \widetilde{S}_{0\perp}\left[\widetilde{\Delta}_{\parallel}\left(A + B\widetilde{S}_{0\parallel}\right) + c_{16}\delta m\right] \tag{2.10}$$

Φ_0 is a stochastic variable that we assume is distributed uniformly in the range $(0, 2\pi)$. The rest of parameters are listed in Table 2.2 (Zlochower & Lousto, 2015).

D	3684.73 ± 5.67 $\mathrm{km\,s^{-1}}$	c_9	-2540 ± 250 $\mathrm{km\,s^{-1}}$
E	0.0705 ± 0.0127	A	2090 ± 210 $\mathrm{km\,s^{-1}}$
F	-0.6238 ± 0.0098	B	4150 ± 690 $\mathrm{km\,s^{-1}}$
c_1	-0.677 ± 0.046	c_{16}	-1280 ± 130 $\mathrm{km\,s^{-1}}$

Table 2.2: Fitting parameters for equations (2.8), (2.9) and (2.10), as provided in Zlochower & Lousto (2015)

The angle ξ was initially modeled as a constant value ($\xi \sim 145°$; Baker et al., 2008; Lousto & Zlochower, 2009; Lousto et al., 2010a,b; Zlochower et al., 2011;

Lousto et al., 2012; Lousto & Zlochower, 2013). Healy et al. (2014) proposed the following formulation based on a larger suite of NR simulations and improved modeling,

$$\xi = a + b\widetilde{S}_{\parallel} + c\delta m\widetilde{\Delta}_{\parallel}\,. \tag{2.11}$$

This is the functional form we adopt in this work, with parameters $a = 2.489240 \pm 0.007421$ rad, $b = 1.428658 \pm 0.035542$ rad and $c = -0.558505 \pm 0.052263$ rad (Healy & Lousto, 2018).

Finally, it worth commenting on the family of non-analytic, so called “surrogate models" for velocity kick (Varma et al., 2019a,b). While free parameters of analytic models are usually calibrated with NR simulations, surrogate models are trained against actual simulations and do not need to introduce additional assumptions. Studies show that they are highly accurate and almost indistinguishable from NR simulations in the portion of parameter space including $|\vec{\alpha}_1|, |\vec{\alpha}_2| \leq 0.8$ and $q \geq 1/4$. Since we are interested in exploring a substantially wider range of the BBH parameter space, we make a choice not to use the surrogate models. This choice is worth revisiting in the future, once the surrogate models are extended to cover a wider portion of the parameter space.

Chapter 3

RALPH: The Algorithm for Analysis of the Gravitational Wave Recoil

In this section we introduce the algorithm developed for analysis of the GW recoil: Recoil Analyzer for Limiting Parameters of binary black Holes (RALPH). As mentioned previously, the analysis of GW signals from merging BBHs is used to infer the properties of the binaries. The outcome of this type of analysis is reflected in the number of BBH parameters that can be measured or constrained, as well as their associated measurement error. These in turn depend on the myriad of factors that affect the signal-to-noise of the measurement including (a) properties intrinsic to the binary (like it mass ratio and spins), (b) extrinsic properties like its distance, location and orientation on the sky, and (c) sensitivity of the detector.

In general, the higher the signal-to-noise ratio of a GW detection, the higher the chances that parameter estimation will return multiple BBH parameters and with a higher precision. Some BBH parameters will require higher signal-to-noise detection to be measured than others and one for example may expect that the BBH mass ratio will be easier to determine than the BH spins, on average. From the two BH spins, the spin of the more massive BH will be easier to infer than that of the lower mass BH.

With this in mind we constructed an algorithm that uses as input the radial velocity, measured from the EM observations, and a limited set of BBH parameters and their uncertainties, likely to be estimated from the GW analysis. The main task of the algorithm is to determine in which BBH configurations a combination of EM and GW measurements leads to an improved estimate of BBH parameters. Here, the improvement constitutes a measurement of an additional, previously unconstrained,

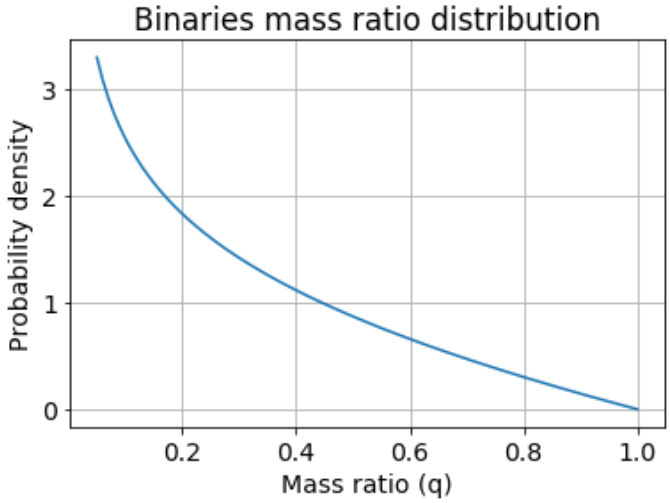

Figure 3.1: Distribution of BBH mass ratios from Hopkins et al. (2010).

BBH parameter as well as the improvement in the precision of a measurement.

Since we account for measurement uncertainties in the recoil velocity and input BBH parameters, all are expressed as intervals. The algorithm produces two different outputs: 1) a portion of the BBH parameter space that is consistent with the specified input parameters and 2) statistical properties of that region of the parameter space. For example, the range and distribution of a parameter, the maximum velocity kick or a measure of how well is the parameter constrained with such priors.

One necessary ingredient for our statistical analysis are prior distributions for the input parameters. The underlying distributions of properties assumed for BBH systems will represent the configuraions of binaries that can in principle be observed by both EM and GW observatories. We briefly introduce some common parameter distributions from the literature that are used in this work.

We consider the mass ratios in the range $q \in [1/20, 1]$ and adopt the distribution from Hopkins et al. (2010), where $f(q) \propto q^{-0.3}(1-q)$. This distribution is shown in Figure 3.1. Similarly, we describe the spin magnitudes and orientations using parameters $a_i \in [0, 1]$, $\theta_i \in [0, \pi]$, and $\varphi_i \in [0, 2\pi]$. We define their distributions following the approach of Lousto et al. (2012), who studied the evolution of the spins in hot and cold disks. They find that in hotter and geometrically thicker disks, nearly isotropic accretion onto BHs leads to weaker spin alignment with the angular momentum of the accretion flow than in cold disks. This results in different

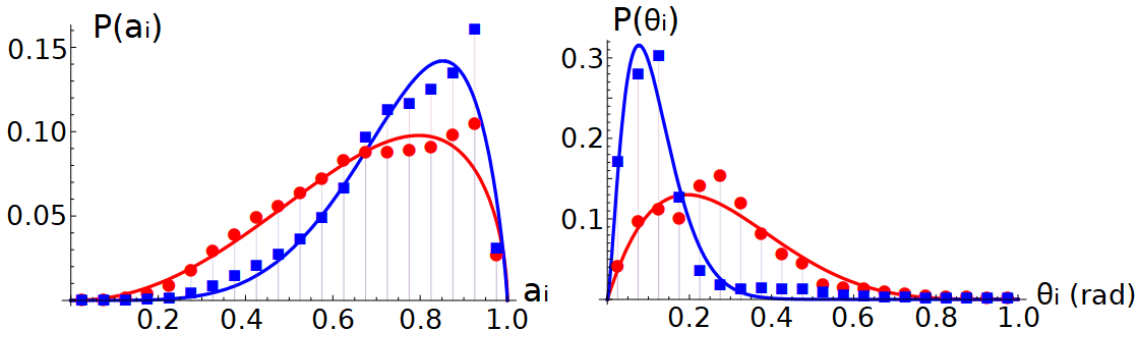

Figure 3.2: Probability that the dimensionless spin of a BH has a given magnitude a_i (left) or a polar angle θ_i (right) for BHs in cold disks (blue squares) and hot disks (red circles). Figure adapted from Lousto et al. (2012).

statistical distributions of spin magnitudes and orientations, as shown in Figure 3.2. These are modeled as beta distributions, i.e. $f(x) \propto \text{Beta}(\alpha, \beta) \propto (1-x)^{\beta-1}x^{\alpha-1}$ with the parameters listed in Table 3.1.

	Spin magnitude (a_1, a_2)		Spin polar angle (θ_1, θ_2)	
	α	β	α	β
Hot disks	3.212 ± 0.258	1.563 ± 0.093	2.018 ± 0.181	5.244 ± 0.604
Cold disks	5.935 ± 0.642	1.856 ± 0.146	2.544 ± 0.198	19.527 ± 2.075

Table 3.1: Parameters for the hot and cold disk models from Lousto et al. (2012).

We consider three different models: 1) the isotropic model, corresponding to the uniform probability of mass ratios and spin magnitudes, and isotropic distribution of spin orientations, 2) the hot disk model with distributions for mass ratios and spins given by the hot disk model. And 3) the cold disk model with distributions for mass ratios and spins given by the cold disks model.

Note that these distributions do not specify the spin orientations in the orbital plane of the binary, measured by azimuthal angles φ_i. Dependence on φ_i is encapsulated in the spin-related variables $\widetilde{\Delta}_\perp$, $\widetilde{S}_\perp$ and $\widetilde{S}_{0\perp}$ (discussed in section 2.3). Since they are the modulus of 2-dimensional vectors, the absolute orientation of the perpendicular components of the BH spins is not important but their relative orientation with respect to one another is. Namely, the dependance of these properties on φ_1 and φ_2 corresponds to dependance on $\varphi_1 - \varphi_2$. Therefore, we assume that φ_1 and φ_2 have uniform distribution in all scenarios. In the analytic kick model we use, the information about the absolute orientation of spins is encoded in the stochastic variable Φ_0. The kick model is thus, non-deterministic. For a more detailed

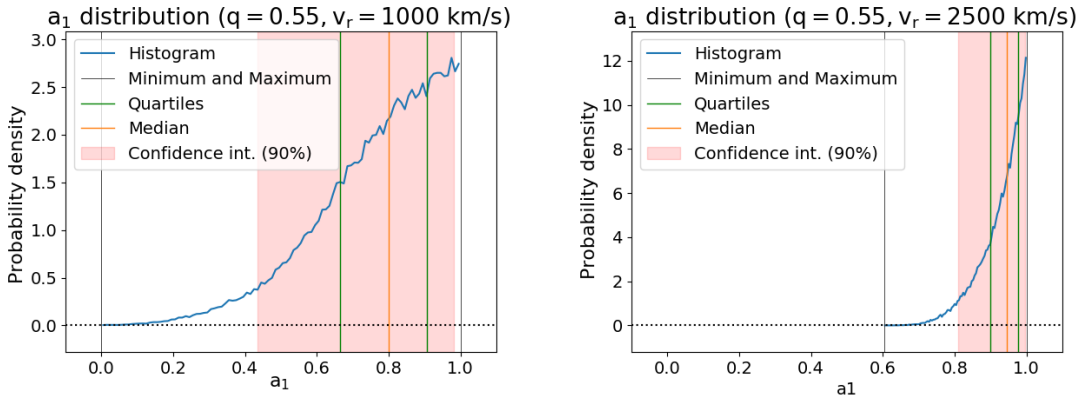

Figure 3.3: Distribution of a_1 assuming $q = 0.55$ and the observed kick velocity $v_r = 1000$ km/s (left panel) and 2500 km/s (right).

explanation of the algorithm, see Appendix A.

The uncertainties associated with priors in our calculations will be based on the expected parameter estimation accuracy of LISA (Klein et al., 2016). According to these expectations, we will adopt $\pm 1\%$ interval for the value of q and $\pm 10\%$ for the values of a_1 and a_2. In scenarios where we examine the orientation of the binary orbit on the sky, we will specify the inclination of the orbit (given by the vector of orbital angular momentum) with respect to the observer's line of sight with the assumed uncertainty of $\pm 1^\circ$. We will assume the uncertainties associated with a measurement of the kick velocity of ± 250 km s^{-1}. This is representative of uncertainties commonly encountered in spectroscopic searches for gravitationally bound SMBH binaries and recoiling SMBHs (Eracleous et al., 2012). Because the radial velocity is a projection of the total kick velocity, it represents a lower limit on its value. For this reason, we refer to the value v_r in the interval $[v_r, v_r + 500$ km s$^{-1}]$.

Our simulations have $N = 10^4$ or $N = 10^5$ realizations for different values the kick velocity and BBH parameters. Using results of these realizations we construct distributions for the region of the parameter space matching the priors. Figure 3.3 shows two examples of probability distributions calculated using this procedure. In this case, we assume that the mass ratio of the binary is $q = 0.55$ and that the observed velocity kick is either $v_r = 1000$ km s^{-1} or 2500 km s^{-1}. We find that in the first case the value of the spin parameter a_1 remains unconstrained between the minimum and maximum value 0 and 1.0, respectively. In the second case, the allowed range of values for a_1 is between 0.6 and 1.0, and is therefore reduced to 40% of its full range.

The examples considered above indicate that the higher observed kick velocities provide stronger constraints on a_1. For any given observed kick velocity we can therefore calculate how well it constraints a given parameter. For example, Figure 3.4 shows the level of constraint placed on a_1 given $q = 0.55$ for different values of v_r. The observed kick velocity of $v_r = 3631$ km s^{-1} allows one to measure the value of a_1 within 10% of its full range.

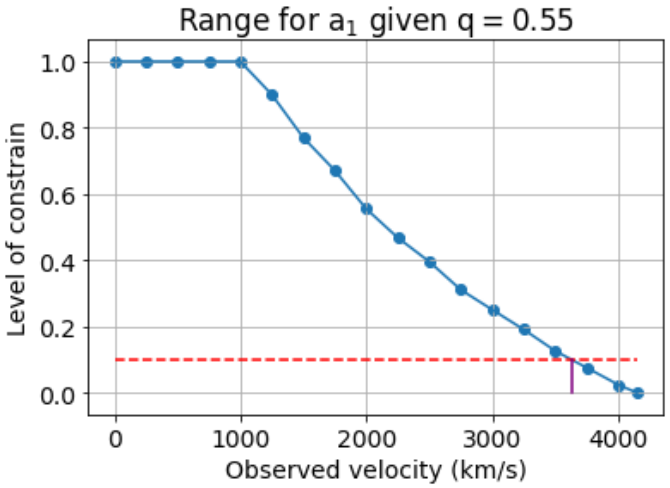

Figure 3.4: Level of constraint placed on a_1 as a function of v_r given $q = 0.55$. The blue points represent the data from our simulations, the blue line is a linear interpolation, and the dashed red line marks the constraint level of 10%.

Chapter 4

Results

4.1 Case 1: Constraining a_1 given the value of q

The first case we consider is also the simplest, as the assumed priors involve a single parameter, the binary mass ratio q. The parameters of this case study are summarized in Table 4.1.

	Parameter	**Values**	**Uncertainty**
Input parameters	q	$0.05, 0.1, \ldots, 0.95, 1.0$	$\pm 1\%$
Observed velocity	v_r	$0, 250, \ldots, 4750$ km/s	± 250 km/s
Output parameter	a_1	-	-

Table 4.1: Parameters in case study 1.

In Figure 4.1 we show the the observed kick velocity v_r that leads to the level of constraint of 10%, 30% and 50% for a_1 as a function of q. Note that the value at $q = 0.55$ corresponds to 3600 km/s at the 10% constraint level, as shown in Figure 3.4 in the previous section. In the same figure, the 30% and 50% constraint levels correspond to lower v_r, specifically, 2800 $\mathrm{km\,s^{-1}}$ and 2150 $\mathrm{km\,s^{-1}}$ respectively. Thus, as noted before, higher kick velocities provide stronger constraints on the value of a_1.

It is then relevant to consider the probability that higher kick velocities will be observed relative to lower ones. To address this question, we use the three models introduced in chapter 3. For each case we use 10^7 realizations with the same input parameters but make no prior assumptions about the observed kick velocity. We then calculate which fraction of BBH configurations reaches a given kick velocity.

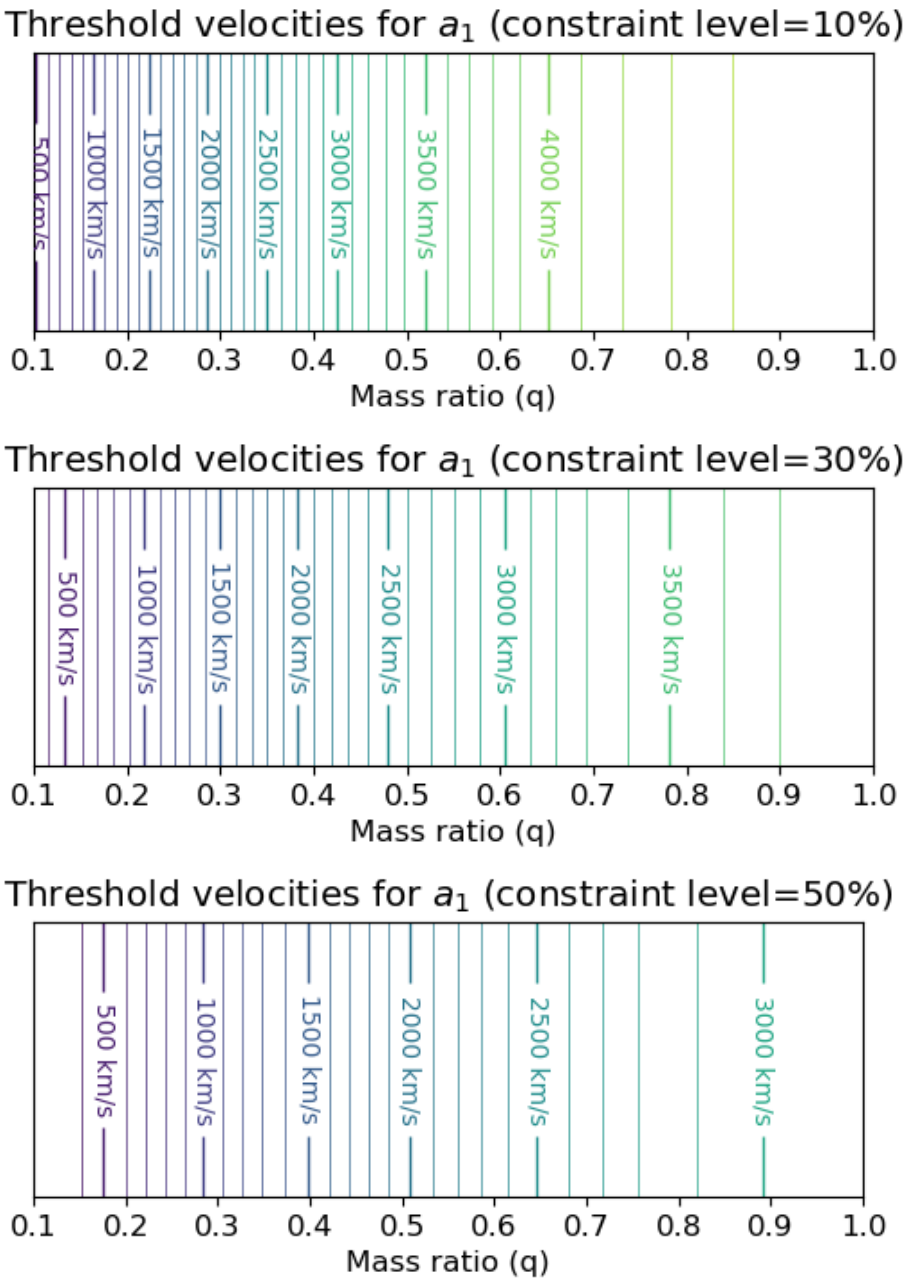

Figure 4.1: Observed kick velocity necessary to constrain a_1 within 10%, 30% or 50% of its full range.

Figure 4.2 shows the probability for observation of the kick velocity necessary to constrain a_1 within 10%, 30%, 50% of the full range of values, between 0 and 1.0. The probabilities shown in these figures take into account the projection effects, as the velocity vector of the remnant BH can have arbitrary orientation relative to the observer's line of sight.

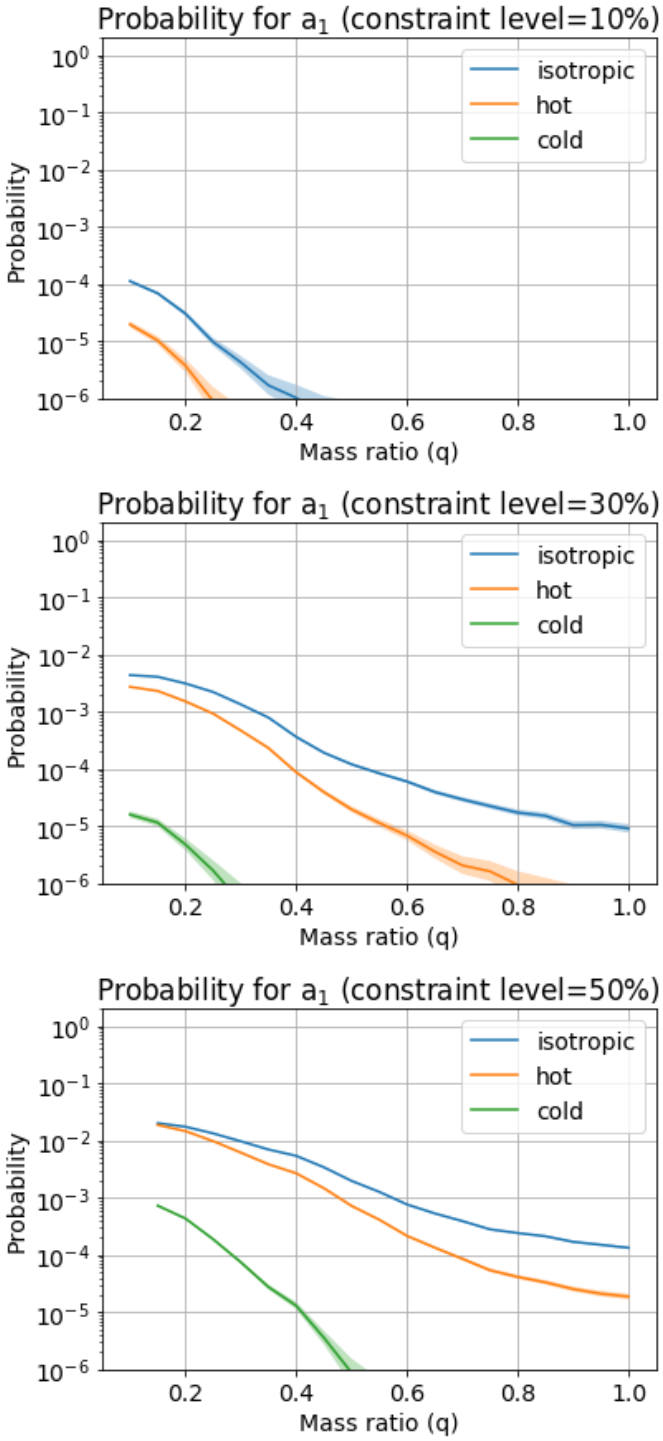

Figure 4.2: Probability of observing the kick velocity required to constrain a_1 within $\Delta a_1 = 0.1$ (top panel) 0.3 (middle) or 0.5 (bottom), anywhere between 0 and 1.0. Shadowed regions mark 90% confidence intervals.

Figure 4.2 indicates at most 10^{-4} merger detections are going to be able to constrain a_1 within 10% if the BH spins are isotropic and their magnitudes uniformly distributed between 0 and 1. This probability drops to about 10^{-5} in the case of the hot disk model and is even lower for the cold disk model. Such low probabilities indicate that it is difficult to decouple high kicks from specific values for a_1, therefore suggesting that there are other important parameters determine the kick velocity. This effect is more visible for comparable mass systems than for more unequal mass systems. This picture changes when one tries to constrain a_1 within broader margins. The odds of placing a constrain to a_1 within 50% using the combination of EM and GW measurements will require about 10^2 multimessenger detections of BBH mergers for the isotropic and hot disk models and more than 10^3 for the cold disk model.

4.2 Case 2: Constraining a_2 given q and a_1

In the next scenario we consider whether any constraints can be placed on the spin magnitude of the secondary BH, a_2, given prior measurements of q and a_1. The parameters of this case study are summarized in Table 4.2. Most of the simulations presented here are based on $N = 10^5$ realizations but some (less than 20%) have $N = 10^4$ or $N = 10^3$ due to their low sampling efficiency (see Appendix A for discussion).

	Parameter	**Values**	**Uncertainty**
Input parameters	q	$0.05, 0.1, \ldots, 0.95, 1.0$	$\pm 1\%$
	a_1	$0.0, 0.2, \ldots, 0.8, 1.0$	$\pm 10\%$
Observed velocity	v_r	$0, 250, \ldots, 4750$ km/s	± 250 km/s
Output parameter	a_2	-	-

Table 4.2: Parameters in case study 2.

We calculate the kick velocities that, if observed, could constrain a_2 within 30% and show them in Figure 4.3. In this case, the figures are 2D plots with the mass ratio on the horizontal axis and primary BH spin magnitude on the vertical axis. For example, given a prior information of $q = 0.7$ and $a_1 = 0.6$, the radial velocity that one needs to observe to constrain a_2 within 0.3 is almost 2600 km s^{-1}. On the top of the 2D figure we also show a 1D panel, reflecting the threshold kick velocity as a function of q only, when no measurement of a_1 is available. This is analogous to the setup in case study 1, except that here we are considering a_2 instead of a_1.

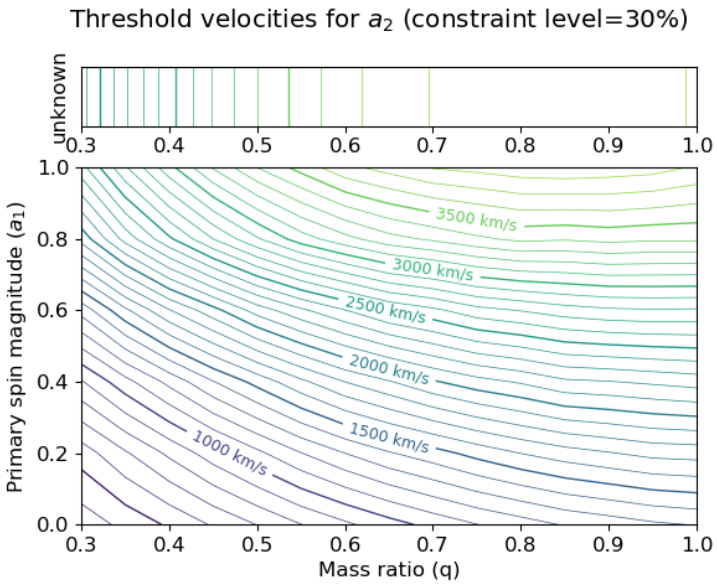

Figure 4.3: Observed kick velocity necessary to constrain a_2 within 30%, such that $\Delta a_2 = 0.3$. The top panel shows the scenario when only q is known and the bottom panel shows the scenario when a priori measurements of both a_1 and q are available.

The contour lines continuity between the two panels of Figure 4.3 indicate that knowing $a_1 = 1.0$ and q is equivalent to only knowing q, in terms of the kick velocity needed to constrain a_2. In general, for all values of a_1 and q, knowing a_1 is beneficial for constraining a_2. We also compare the top panel with Figure 4.1 in case study 1. The comparison shows that higher kick velocities are required to constrain a_2 within the same range as a_1, for the same mass ratio prior. The exception are configurations with $q \approx 1$, where both the primary and secondary spin contribute to the total spin with comparable weight. In this case the value of the kick velocity necessary to achieve measurements with precision $\Delta a_1 = \Delta a_2 = 0.3$ is comparable for a_1 and a_2.

Figure 4.4 shows the detection probability of remnant BH with velocity such that it constrain a_2 within 30%, when only q is used as a prior and a_1 is not known. As we mentioned above, this setup is similar to the case study 1, but now the output parameter is a_2 instead of a_1. In this case, given the same mass ratio and scenario, constraining a_1 is easier than constraining a_2. Similarly, both cases converge to the same probability of constraining the spin magnitude when $q = 1$. This feature highlights the fact that a_1 and a_2 are interchangable in the case $q = 1$ as the two BHs have the same mass.

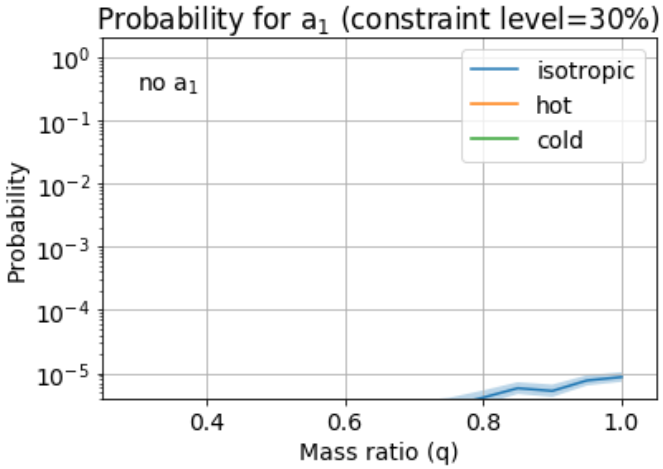

Figure 4.4: Probability of observing the kick velocity required to constrain a_2 within 30% of its full range, given prior knowledge of q but no knowledge of a_1. Shadowed region marks 90% confidence interval.

We now consider the probability for such kick velocities to be observed, given prior knowledge of both q and a_1, as well as arbitrary orientation of the velocity vector to the observer's line of sight. In Figure 4.5 we show the probability that a_2 can be constrained at the levels of 30% in different configurations. We find a preference for the isotropic model as the most promising scenario, followed by the hot disk model. We also highlight a trend with q: the higher the mass ratio, the easier it is to constrain a_2. This can be understood, as the higher q, the more massive the secondary BH, so the more important is its spin contribution for the resulting kick velocity.

The second trend we identify is with respect to a_1. In general, the lower the value of a_1, the easier it is to constrain a_2. This indicates that for low a_1, a_2 is more important in the kick models. This effect is most noticeable for low mass ratios. One can understand this as the contribution of a_2 in low mass ratio binaries is less important unless a_1 is low. We also find that the impact of a_1 on the probability for measurement of a_2 is more important than that of q. In summary, the most promising configurations for measurement of a_2 are those with low a_1. Achieving the level of constraint of 30% is going to require about than 10^3 joint detections for all but the lowest values of a_1.

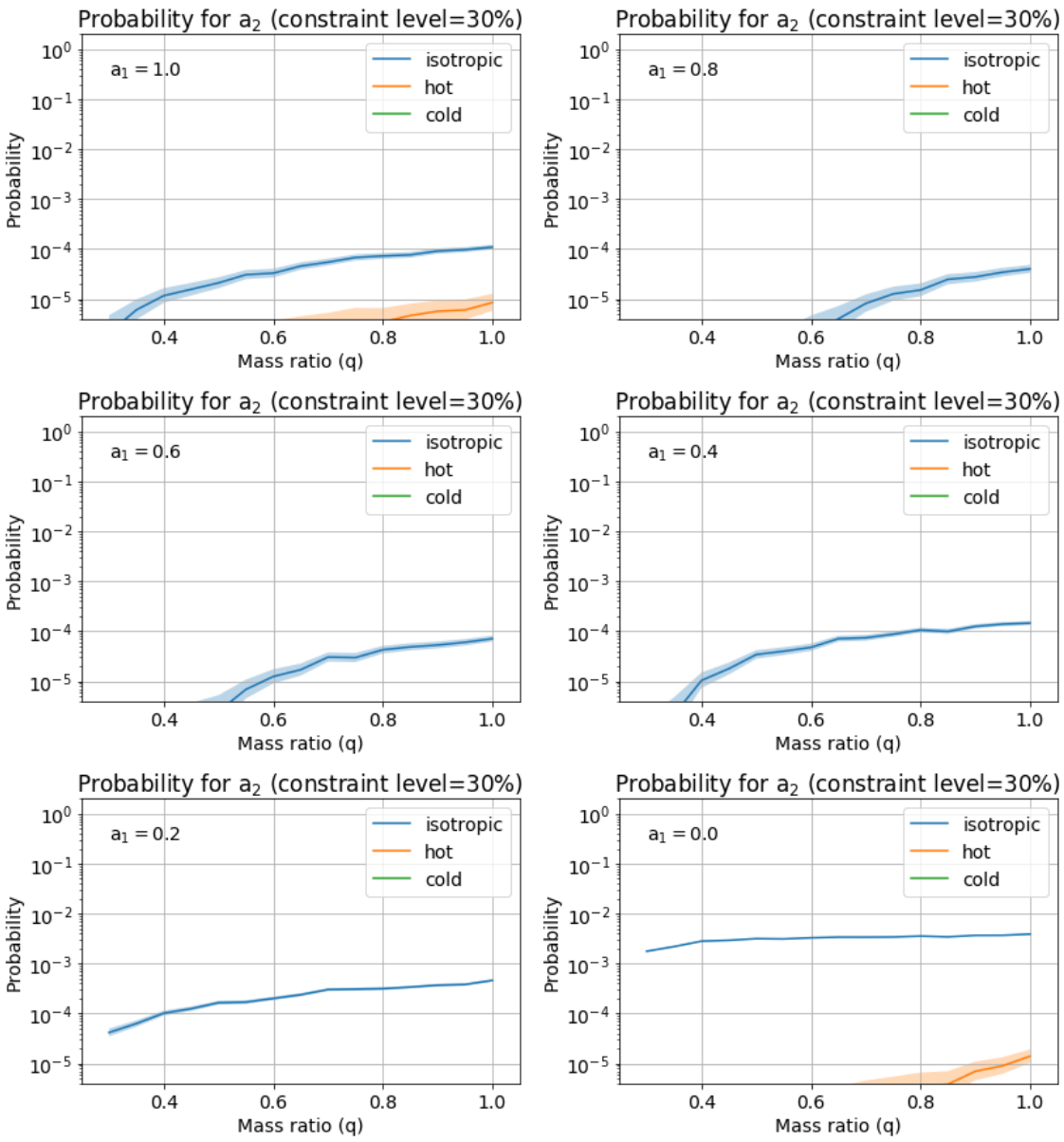

Figure 4.5: Probability of observing the velocity required to constrain a_2 within $\Delta a_2 = 0.3$ as a function of q and a_1. Shadowed regions mark 90% confidence intervals.

4.3 Case 3. Constraining a_1 and a_2 given q and binary inclination, β

The third and last case study examines the hypothesis that knowing the binary orbital inclination could help in the parameter estimation. Equation (4.1) illustrates that prior knowledge of β provides an upper bound to the kick velocity, in addition to the lower bound which can be placed even when β is not known.

$$v_{\parallel} \cos\beta - v_{\perp} \sin\beta \leq v_r \leq v_{\parallel} \cos\beta + v_{\perp} \sin\beta \tag{4.1}$$

In what follows, we are going to investigate whether added knowledge of the upper bound on v_r can inform parameter estimation in any useful way. We list the parameters for this case study in Table 4.3.

	Parameter	**Values**	**Uncertainty**
Input parameters	q	$0.05, 0.1, \ldots, 0.95, 1.0$	$\pm 1\%$
	β	$0, 10^\circ, \ldots, 80^\circ, 90^\circ$	$\pm 1^\circ$
Observed velocity	v_r	$250, 500, \ldots, 5000$ km/s	± 250 km/s
Output parameters	a_1, a_2	-	-

Table 4.3: Parameters in case study 3.

We use $N = 10^4$ realizations for each (q, β, v_r) configuration. We present the results in Figure 4.6 for a_1 and a_2 respectively. Both figures show the observed kick velocity necessary to constrain the spin magnitudes within 30% (or 0.3) of the full range of values from 0 to 1.0. The 1D panels show the kick velocity needed to obtain the same level of constraint if only q is known. Note that these are identical to 1D plots shown at the top of Figure 4.1 in case study 1 and Figure 4.3 in case study 2.

Inspection of Figure 4.6 shows that the contours in 1D and 2D panels no longer are aligned for a given q. Specifically, the kick velocities in 1D panels are larger than for any value of β in the 2D panel. For example, for $q = 0.6$ and no prior knowledge of β, the threshold velocity is near 3000 $\mathrm{km\,s^{-1}}$ in the panel describing the measurement of a_1. With the prior knowledge of $\beta = 0^\circ$ however, it is just above 2700 $\mathrm{km\,s^{-1}}$, and keeps decreasing to less than 300 $\mathrm{km\,s^{-1}}$ for $\beta = 90^\circ$. We therefore conclude that knowing the binary inclination always improves the measurement of the spin. This is a first hint that knowing the binary inclination as a prior will be the key to make the most of joint GW and EM detections.

It is worth noting that in Figure 4.6 the contours in the region of $\beta > 70^\circ$ tend to be more noisy. This is due to uncertainties in the calculation method that are larger

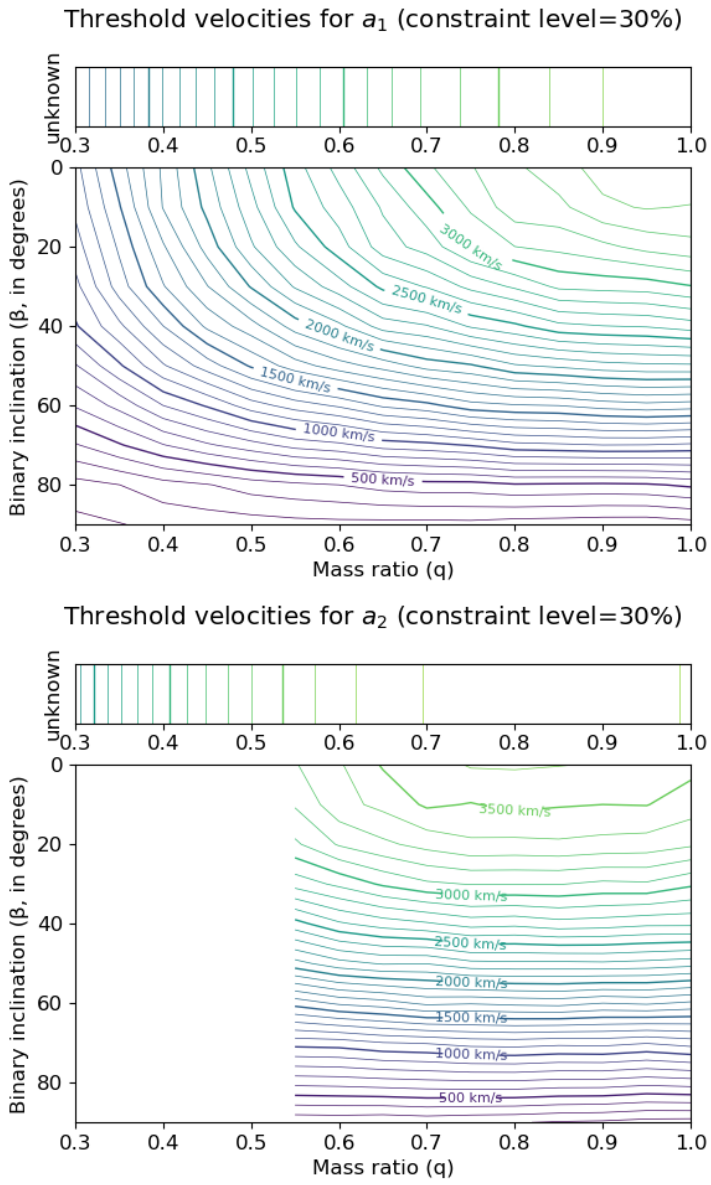

Figure 4.6: Observed kick velocity needed to constrain a_1 (top) and a_2 (bottom) within 30% of its full range of values (i.e., $\Delta a_1 = \Delta a_2 = 0.3$).

for this region of the parameter space. A similar effect happens for $q < 0.55$ in panel for a_2, in which we do not draw contours to avoid extrapolation from incomplete data.

Examining the trend with β, one can see that for binaries which orbit is oriented edge-on to the observer's line of sight ($\beta \sim 90°$), the required radial velocities are fairly low, and in the ballpark in which recoil measurements are of the same order

of their own uncertainties. This implies that even a low recoil velocity measurement may be informative. This also manifests clearly that the larger component of the recoil kick is parallel to the orbital angular momentum, since projections with $\beta \sim 0^\circ$ show the full component, while projections with $\beta \sim 90^\circ$ supress it.

As before, we evaluate the probability for a remnant BH to achieve these kick velocities, in order to understand how many joint EM and GW detections would be needed before one can constrain a_1 and a_2 with a desired precision. Figures 4.7 and 4.8 show the probability that a_1 and a_2 can be constrained within 30% of the full range of values, respectively. Comparing these figures, we note the same trends we have introduced earlier in this section: for a_1 the probability grows wth decreasing q, in the way opposite from a_2. Similarly, constraining a_2 is much harder than a_1 for all mass ratios, except for $q \approx 1$, when the probabilities of these two measurements are comparable.

Trends with β vary for different models. While in the hot disk model we observe higher probabilities the lower the binary inclination, for the isotropic, probabilities remain quite similar in all cases, jumping up almost an order of magnitude when the binary is edge-on. This confirms our expectation that edge-on binaries will benefit the most from the multi-messenger approach in terms of their parameter estimation.

In summary, our results indicate that in scenarios when prior knowledge of q and β is available, at least 10^2 joint EM and GW detections will be needed to constrain a_1 within a 30%. The best chance of measuring a_2 is for configurations with equal-mass binaries and edge-on binaries, where at least 10^3 joint detections will be needed to constrain a_2 within a 30%.

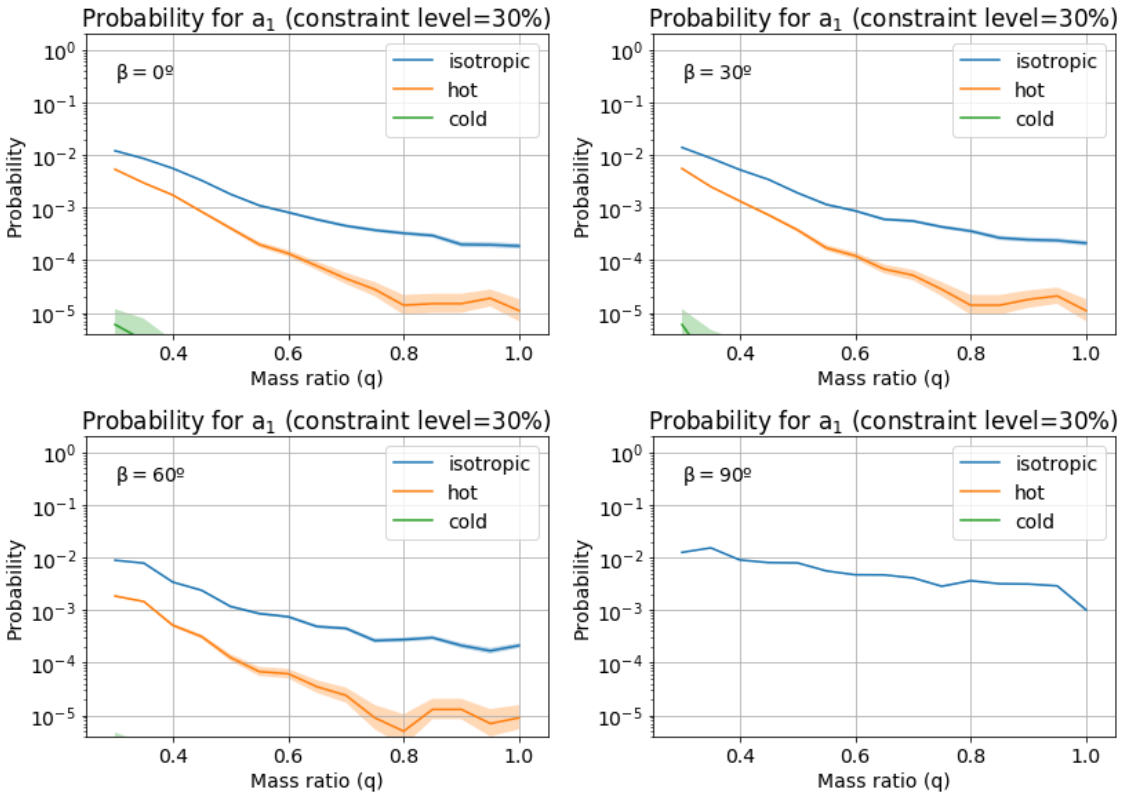

Figure 4.7: Probability of observing the kick velocity required to constrain a_1 within 30%. The corresponding value of β is marked in each panel. Shadowed regions are 90% confidence intervals.

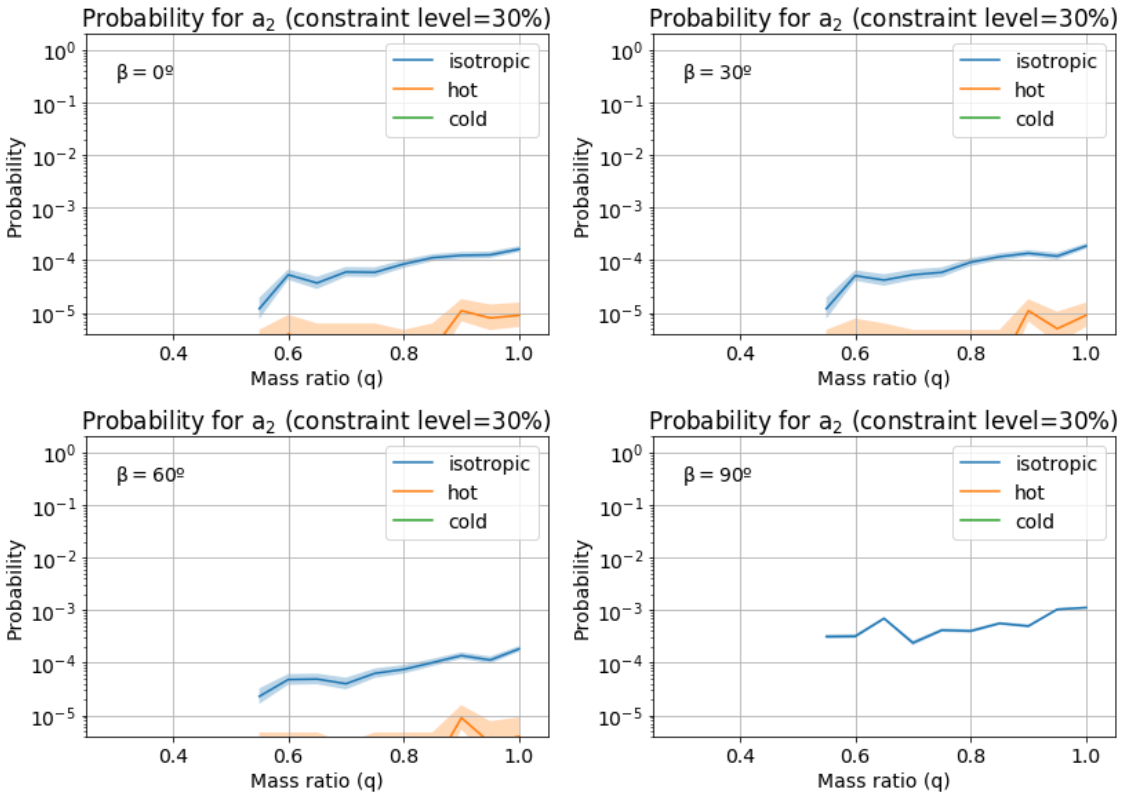

Figure 4.8: Probability of observing the kick velocity required to constrain a_2 within 30%. The corresponding value of β is marked in each panel. Shadowed regions are 90% confidence intervals.

Chapter 5

Discussion

In this thesis we evaluate the power of multimessenger astronomy in the case of merging BBHs. We have quantified how useful multimessenger detections can be, given several physically motivated scenarios. We have presented the radial velocities that are necessary to obtain useful constraint levels on the BH spins, and calculated probabilities to obtain such measurements.

The outcome we find depends highly on the model chosen to describe the prior distributions of the binary parameters. With the spin distributions predicted by the cold disk model, probabilities of having useful kicks are in most cases too low to be interesting, reaching at most $\sim 10^{-3}$ for a 50% level of constraint. This implies that in the cold disk model more than 10^3 joint EM and GW detections must be made before one can hope to place this level of constraint on SMBH spins.

The hot disk model gives more favorable results, since the probabilities are always higher than in the cold disk model, all other things being the same. The most promising however is the isotropic model, with probabilities reaching 10^-2, indicating that $\sim 10^2$ combined detections may be enough to place a useful constraint on BH spins. Unlike the cold and hot disk models, one may expect SMBHs to have an isotropic distribution of spins in astrophysical scenarios in which accretion onto the BHs is either unimportant or is more or less isotropic. In that case, there would be no preferred angular momentum axis imposed by the gas accretion flow and the evolution of BH spin orientations and magnitudes though cosmic history would be stochastic and driven by mergers with other BHs. Therefore, in order to understand which of the models is most relevant to SMBHs, it is crucial to understand the evolution of the SMBH binary systems, as well as the environments that they live in.

In the probabilities plots we calculate the odds of constraining the output parameter within the constraint level, in the scenario specified by the input parameters. If probabilities are high, this means that the output parameters is a more important factor for the total kick $v_{\rm kick}$, while low probabilities indicate that the effect of the output parameter in the kick is weak.

It may seem surprising that probabilities are so low in some cases that do not even appear in some graphs. For example, in Figure 4.5, realizations of input parameters using the cold disk model reach the expected radial velocities with a probability lower than 10^{-6}. Low probabilities may be caused by three different effects: 1) the kick only weakly depends on a given parameter. Then, it's nearly impossible to constrain it by measuring the radial velocity, as the kick is virtually independent from that parameter. 2) The kick models are also not fully deterministic, due to the fact that the azimuthal orientation of the BH spins (encoded in variable Φ_0) is not known. Therefore, even that the input parameters are appropriate for a kick to overcome the threshold, it will not succeed all the times, and 3) projection issues play a role, since even if the remnant BH is recoiling at a velocity over the threshold, the kick may be oriented in a direction such that the radial velocity measured by a distant observer is less than the threshold.

Using recoil measurements to do parameter estimation requires observations. As discussed in the introductory chapter, such observations need the BH to be active, and therefore more likely be in a gas-rich environment. These environments tend to give rise to aligned BH spins, as in hot and cold gas disk models. In fact, the best test for our results will be to compare the expected probability of having such recoil with real observations. This will test both our model and the previous assumptions on the underlying distributions.

In the case of the cold disk model, the probabilities of observing the threshold velocities are too low to be of practical interest. This is due to the strict alignment of the spins, that leaves no room for high kicks. The algorithm could in principle be modified by effectively ruling out this portion of the parameter space from the get-go. This would result in more realistic threshold velocities, since the highest kicks would be impossible to observe in such scenario.

Our model only considers BBH configurations with mass ratios $q \geq 1/20$. The configurations with $q < 1/20$ have GW kicks lower than 300 $\mathrm{km\,s^{-1}}$, that are comparable or lower than the expected measurement uncertainties of the recoil velocity. Therefore, not considering such low mass ratios does not affect our results, as such recoil velocities would be difficult to measure in practice.

An important characteristic of our results has to do with the level of constraint. It is worth noting that we use the algorithm described here to calculate the relative improvement in measurement of a given property (a_1 or a_2) given joint EM and GW observations. We however do not discuss the most likely values of a_1 or a_2 calculated by the algorithm, even though the algorithm has the capability to make such predictions. For example, when we constrain a parameter (e.g., a_1) up to a 10% of its original range, we know it is constrained within $\Delta a_1 = 0.1$ but we do not know whether this interval is $[0, 0.1]$, $[0.53, 0.63]$ or any other interval inside $[0, 1.0]$. We know nevertheless that dependence of the kick velocity on the spin magnitude is almost always monotonous and increasing, and the highest kicks for the same spin orientation are achieved when the spin magnitude is maximal. This indicates that when we refer to constraint level 10%, the interval is effectively $[0.9, 1]$ and when the level of constraint is 50%, the interval is indeed $[0.5, 1]$. We need to be very careful to not generalize, since for spin inclination θ_i we do not know where will the level of constrain (now measured in terms of π rad) be inside the $[0, \pi]$ as the maximum kicks are normally achieved somewhere in between 0 and $\pi/2$, but not always at the same angles.

Having said that, our model is effective in placing lower bounds on spin magnitudes, but probably not as effective in placing upper bounds, and this effect can boost the performance of our algorithm. For example, in the scenario where we have the prior knowledge about the mass ratio and try to constrain a_1 with a recoil velocity measurement, if we knew that $a_1 < 0.6$ we could take the velocities of the 50% level of constrain plot (that successfully places lower bound at $a_1 > 0.5$) to have the spin constrained in an interval of length 0.1, effectively constraining it to 10% level. This means that our algorithm is effective in improving the constraints not only for the parameters that cannot be measured from GWs but also for those that can measured but with poor accuracy.

Chapter 6

Conclusions

In this thesis, we investigate how multi-messenger detections (using both EM and GW signals) of mergers of SMBH binaries can be combined in order to determine the parameters of these systems. We present a computational model to describe how recoil measurements can help to constrain BBH parameters, given some prior knowledge of parameter values from GW analysis. We have also quantified what is the probability that BBH parameters can be improved using multimessenger detections. The main results of this thesis are as follows:

1. Although kicks can reach up to nearly 5000 $\mathrm{km\,s^{-1}}$ and there are a lot of degeneracies involved, kicks as low as 500 $\mathrm{km\,s^{-1}}$ can be useful for parameter estimation in a large number of cases.

2. If we know the mass ratio of the binary, measuring a recoil velocity can help constrain the primary BH spin magnitude. This can be achieved more effectively at lower mass ratios, where one needs to make about 100 multimessenger detections in order to have a chance to place useful constraints on the primary BH spin magnitude.

3. If we know the mass ratio and the primary BH spin magnitude, measuring a recoil velocity can help constrain the secondary BH spin magnitude. This can be achieved more effectively at higher mass ratios, where one needs to make at least $\sim$ few $\times$ 100 multimessenger detections in order to have a chance to place useful constraints on the secondary BH spin magnitude in one such case.

4. Measuring the binary inclination together with the recoil velocity can also help constrain both BH spin magnitudes. This can be achieved more effectively at lower mass ratios, where one needs to make about 100 multimessenger

detections in order to have a chance to place useful constraints on the primary BH spin magnitude in one such case.

5. The useful constraints on BH spins are most likely to be obtained if their spin vectors are isotropically oriented on the sky. If BBH spin vectors are driven to partial alignment with each other and orbital angular momentum by some external process, like accretion from a disk, then observations of binaries in hot disks are far more likely to provide useful constraints than those in cold disks.

With the recent coincident detection of both GW and EM signatures from a NS-NS merger (Abbott et al., 2017) the era of multimessenger astronomy has truly begun. In addition to these, multimessenger detections for SMBH binaries are anticipated in the future and are the next thing to come. Our ability to do parameter estimation will be very important when such detections become available. This work makes a step in that direction by exploring how multimessenger detections of BBHs can enhance our knowledge of these systems by being innovative in its quantitative analysis. The future awaits us.

Bibliography

Abbott, B. P., Abbott, R., Abbott, T. D., et al. 2016, Physical Review Letters , 116, 061102

—. 2017, Astrophysical Journal Letters, 848, L12

—. 2019, Physical Review X, 9, 031040

Amaro-Seoane, P., Audley, H., Babak, S., et al. 2017, arXiv e-prints, arXiv:1702.00786

Baker, J. G., Boggs, W. D., Centrella, J., et al. 2007, Astrophysical Journal , 668, 1140

—. 2008, Astrophysical Journal Letters, 682, L29

Baker, J. G., Centrella, J., Choi, D.-I., et al. 2006, Astrophysical Journal Letters, 653, L93

Begelman, M. C., Blandford, R. D., & Rees, M. J. 1980, Nature, 287, 307

Bekenstein, J. D. 1973, Astrophysical Journal , 183, 657

Berczik, P., Merritt, D., Spurzem, R., & Bischof, H.-P. 2006, Astrophysical Journal Letters, 642, L21

Blecha, L., Brisken, W., Burke-Spolaor, S., et al. 2019, Astro2020: Decadal Survey on Astronomy and Astrophysics, 2020, 318

Blecha, L., Civano, F., Elvis, M., & Loeb, A. 2013, MNRAS , 428, 1341

Blecha, L., Sijacki, D., Kelley, L. Z., et al. 2016, MNRAS , 456, 961

Bogdanović, T. 2015, in Gravitational Wave Astrophysics, Vol. 40, 103

Bogdanović, T., Eracleous, M., & Sigurdsson, S. 2009, Astrophysical Journal , 697, 288

Bogdanović, T., Reynolds, C. S., & Miller, M. C. 2007, Astrophysical Journal Letters, 661, L147

Bonning, E. W., Shields, G. A., & Salviander, S. 2007, Astrophysical Journal Letters, 666, L13

Boylan-Kolchin, M., Ma, C.-P., & Quataert, E. 2008, MNRAS , 383, 93

Brügmann, B., González, J. A., Hannam, M., Husa, S., & Sperhake, U. 2008, Physical Review D , 77, 124047

Brügmann, B., Tichy, W., & Jansen, N. 2004, Physical Review Letters , 92, 211101

Campanelli, M., Lousto, C., Zlochower, Y., & Merritt, D. 2007a, Astrophysical Journal Letters, 659, L5

Campanelli, M., Lousto, C. O., Marronetti, P., & Zlochower, Y. 2006a, Physical Review Letters , 96, 111101

Campanelli, M., Lousto, C. O., & Zlochower, Y. 2006b, Physical Review D , 73, 061501

Campanelli, M., Lousto, C. O., Zlochower, Y., & Merritt, D. 2007b, Physical Review Letters , 98, 231102

Chiaberge, M., Tremblay, G. R., Capetti, A., & Norman, C. 2018, Astrophysical Journal , 861, 56

Chiaberge, M., Ely, J. C., Meyer, E. T., et al. 2017, Astronomy & Astrophysics, 600, A57

Civano, F., Elvis, M., Lanzuisi, G., et al. 2010, Astrophysical Journal , 717, 209

—. 2012, Astrophysical Journal , 752, 49

Dotti, M., Montuori, C., Decarli, R., et al. 2009, MNRAS , 398, L73

Eracleous, M., Boroson, T. A., Halpern, J. P., & Liu, J. 2012, ApJS , 201, 23

Ferrarese, L., & Merritt, D. 2000, Astrophysical Journal Letters, 539, L9

Fitchett, M. J. 1983, MNRAS , 203, 1049

Fitchett, M. J., & Detweiler, S. 1984, MNRAS , 211, 933

Flanagan, É. É., & Hughes, S. A. 1998a, Physical Review D , 57, 4535

—. 1998b, Physical Review D , 57, 4566

González, J. A., Hannam, M., Sperhake, U., Brügmann, B., & Husa, S. 2007a, Physical Review Letters , 98, 231101

González, J. A., Sperhake, U., Brügmann, B., Hannam, M., & Husa, S. 2007b, Physical Review Letters , 98, 091101

Hawking, S. W. 1972, Communications in Mathematical Physics, 25, 152

Hawking, S. W., & Israel, W. 1979, General relativity (Cambridge University Press)

Healy, J., Herrmann, F., Hinder, I., et al. 2009, Physical Review Letters , 102, 041101

Healy, J., & Lousto, C. O. 2018, Physical Review D , 97, 084002

Healy, J., Lousto, C. O., & Zlochower, Y. 2014, Physical Review D , 90, 104004

—. 2017, Physical Review D , 96, 024031

Herrmann, F., Hinder, I., Shoemaker, D., & Laguna, P. 2007a, Classical and Quantum Gravity, 24, S33

Herrmann, F., Hinder, I., Shoemaker, D., Laguna, P., & Matzner, R. A. 2007b, Astrophysical Journal , 661, 430

Hopkins, P. F., Bundy, K., Croton, D., et al. 2010, Astrophysical Journal , 715, 202

Jonker, P. G., Torres, M. A. P., Fabian, A. C., et al. 2010, MNRAS , 407, 645

Kalfountzou, E., Santos Lleo, M., & Trichas, M. 2017, Astrophysical Journal Letters, 851, L15

Kim, D. C., Yoon, I., & Evans, A. S. 2018, Astrophysical Journal , 861, 51

Kim, D. C., Yoon, I., Privon, G. C., et al. 2017, Astrophysical Journal , 840, 71

Klein, A., Barausse, E., Sesana, A., et al. 2016, Physical Review D , 93, 024003

Komossa, S. 2012, Advances in Astronomy, 2012, 364973

Komossa, S., Zhou, H., & Lu, H. 2008, Astrophysical Journal Letters, 678, L81

Koppitz, M., Pollney, D., Reisswig, C., et al. 2007, Physical Review Letters , 99, 041102

Koss, M., Blecha, L., Mushotzky, R., et al. 2014, MNRAS , 445, 515

Loeb, A. 2007, Physical Review Letters , 99, 041103

Lousto, C. O., Campanelli, M., Zlochower, Y., & Nakano, H. 2010a, Classical and Quantum Gravity, 27, 114006

Lousto, C. O., Nakano, H., Zlochower, Y., & Campanelli, M. 2010b, Physical Review D , 81, 084023

Lousto, C. O., & Zlochower, Y. 2008, Physical Review D , 77, 044028

—. 2009, Physical Review D , 79, 064018

—. 2011a, Physical Review Letters , 107, 231102

—. 2011b, Physical Review D , 83, 024003

—. 2013, Physical Review D , 87, 084027

Lousto, C. O., Zlochower, Y., Dotti, M., & Volonteri, M. 2012, Physical Review D , 85, 084015

Markakis, K., Dierkes, J., Eckart, A., et al. 2015, Astronomy & Astrophysics, 580, A11

Merritt, D., Milosavljević, M., Favata, M., Hughes, S. A., & Holz, D. E. 2004, Astrophysical Journal Letters, 607, L9

Milosavljević, M., & Merritt, D. 2003, Astrophysical Journal , 596, 860

Peres, A. 1962, Physical Review, 128, 2471

Pollney, D., Reisswig, C., Rezzolla, L., et al. 2007, Physical Review D , 76, 124002

Pretorius, F. 2005, Physical Review Letters , 95, 121101

—. 2007, arXiv e-prints, arXiv:0710.1338

Richstone, D., Ajhar, E. A., Bender, R., et al. 1998, Nature, 385, A14

Robinson, A., Young, S., Axon, D. J., Kharb, P., & Smith, J. E. 2010, Astrophysical Journal Letters, 717, L122

Ryu, T., Perna, R., Haiman, Z., Ostriker, J. P., & Stone, N. C. 2018, MNRAS , 473, 3410

Schmidt, P., Ohme, F., & Hannam, M. 2015, Physical Review D , 91, 024043

Schnittman, J. D. 2007, Astrophysical Journal Letters, 667, L133

Stanek, K. Z., Kochanek, C. S., Bersier, D., et al. 2019, The Astronomer's Telegram, 12794, 1

Varma, V., Field, S. E., Scheel, M. A., et al. 2019a, Physical Review Research, 1, 033015

Varma, V., Gerosa, D., Stein, L. C., Hébert, F., & Zhang, H. 2019b, Physical Review Letters , 122, 011101

Vivek, M., Srianand, R., Noterdaeme, P., Mohan, V., & Kuriakosde, V. C. 2009, MNRAS , 400, L6

Zlochower, Y., Campanelli, M., & Lousto, C. O. 2011, Classical and Quantum Gravity, 28, 114015

Zlochower, Y., & Lousto, C. O. 2015, Physical Review D , 92, 024022

Appendices

Appendix A

RALPH step by step

The algorithm uses the input information (observed kick velocity and prior knowledge of BBH parameters) to determine the region of the parameter space occupied by BBH configurations consistent with the kick velocity and to evaluate the probability with which such configurations arise. The calculation performed by the algorithm can be split into three main steps: (1) defining the parameter space, (2) identifying the region of relevance and calculating many realizations of BBH configurations, and (3) studying the probability for BBH configurations.

A.1 Step I: Defining the parameter space

The parameter space we are dealing with consists of the independent intrinsic parameters of the binary: mass ratio and spin vectors for both BH. Hence, it is a 6-dimensional parameter space, since we already discussed in section 3 that we can condense φ_1 and φ_2 into $\varphi_1 - \varphi_2$. This process of defining the parameter space only needs to be done once, unless it is necessary to change the resolution of the cubes (which should not change the results).

The first step is the **grid setting**, that has the goal of dividing the parameter space into small hypercubes:

1. Establish the number of partitions in each dimension: N_q (for q), N_a (for a_1, a_2), N_t (for θ_1, θ_2) and N_p (for $\varphi_1 - \varphi_2$).

2. Construct $N = N_q {N_a}^2 {N_t}^2 N_p$ hypercubes. They should all have the same probability, therefore the limits of the cubes depend on the corresponding number of partitions and the chosen model (isotropic, hot or cold disk). For

example, in the case of the isotropic model, the partitions are uniform in $q, a_1, a_2, \cos\theta_1, \cos\theta_2, \varphi_1 - \varphi_2$.

The second process is the **cube characterization**, that analyzes each and every cube and stores information on it:

3. Examine each and every cube and characterize them. In every cube, store the minimum and maximum values for the 6 coordinate parameters. Compute the values of $\chi_{\rm eff}$, $\chi_{\rm p}$ (see Abbott et al., 2019; Schmidt et al., 2015, for definitions) and maximum kick $v_{\rm kick}$ for all the 2^6 vertices of every hypercube to find the minimum and maximum values over the vertices. We can guarantee that the maximum of such parameters is indeed in a vertex of the cube for all parameters except $v_{\rm kick}$ taking N_p an even number. For the case of $v_{\rm kick}$ we will apply a tolerance, as we explain in the sixth step.

4. Store all these values in a parameter file that will be used in the next step to evaluate whether a cube is consistent with the input information (observed velocity and the known BBH parameters).

Because this process is time and RAM memory intensive, it is preferable to do it once, store the values and use them multiple times to calculating them every thime for a new combination of input parameters.

A.2 Step II: Finding the relevant region and sampling

Remember that the initial conditions may be expressed as intervals for any of the intrinsic parameters $(q, a_1, a_2, \theta_1, \theta_2, \varphi_1 - \varphi_2)$, $\chi_{\rm eff}$, $\chi_{\rm p}$ or the binary orientation β. Any parameter for which an initial condition is specified must fulfill it, by having value inside the specified interval. Any parameter for which no initial condition is specified takes any value inside its valid range.

This is the main section of the algorithm. In this process we input the observed velocity and the known BBH parameters. The output will be an unbiased sample of points in the parameter space matching the input information. This step is subdivided into the following substeps:

5. Import the cube data from the previous phase. Remember that the cubes have uniform probability.

6. Use each cube's characteristics to select it or not by determining whether it contains values consistent with the initial conditions. More specifically, go through each initial condition and check whether it is accomplished in any point of the cube:

   - if the condition is on any parameter except β, check whether the ranging interval of the cube for that specific parameter is consistent with the condition on such parameter. If they are inconsistent, the cube is discarded.
   - if the condition is on β we will ignore at this time and will apply it when we do the sampling.
   - if the condition is on the observed velocity, a cube will only be rejected if the maximum velocity on its vertices is below the minimum of the observed velocity's range. In this case we may apply a tolerance of about a 10% to the maximum velocity on the cube's vertices, to account for the possibility that the maximum kick in that cube is a bit higher than the maximum velocity in the vertices and is located in a point inside the cube.

Once we have checked all the cubes, if at least one was accepted there is hope for the existence of some points in the parameter space fulfilling all the initial conditions and the observed velocity. We now need to do the sampling of such points.

7. Set beforehand the size of such sample N.

8. Sampling process as psuedocode:

```
goodpoints = 0
while goodpoints < N:
    select cube;
    sample a point inside that cube;
    if initial conditions(point) are True:
        add point to sample
        goodpoints++
```

   Remarks on each step:

   - Since all the cubes have the same probability (we have constructed them that way) the cube selection is just a random uniform selection.

- The sampling of a point inside the cube should be done using the parameter distributions from the chosen model (isotropic, hot disk or cold disk), although in the case where the number of cubes is big enough, a uniform sampling would be satisfactory.
- When checking the initial conditions, we do it the same way that when selecting the appropriate cubes with three major differences:
  - When checking the cubes we used the maximum kick on the cube, therefore we were applying $\Phi_0 = 0$ in equation 2.7. Now we are using the (stochastic) kick model. Therefore, if the same point would be sampled twice, it could get two different outcomes, with the condition on the observed velocity rejecting one and accepting the other.
  - There are no tolerances, as each point will be "individually" accepted or rejected.
  - We now account for the binary inclination β by modifying the way in which we check the observed velocity requirement. In the case we don't have an initial condition on the binary orientation, the only restriction we can apply for a point with a kick $v_{\rm kick}$ is to be greater than the minimum of the range of the observed kick v_r (we are observing a projection of such total kick). In the case that we have an initial condition on the binary inclination, i.e. the angle β between the line of sight and the orbital angular momentum of the binary, we can infer crucial information about the projection. We will take advantage of the decomposition of the total kick V into two components $v_\parallel$ and $v_\perp$, that we know are parallel and perpendicular to the orbital angular momentum. We can calculate both of them separately and use the criterion showed in the following equation:

$$v_\parallel \cos\beta - v_\perp \sin\beta \leq v_r \leq v_\parallel \cos\beta + v_\perp \sin\beta \tag{A.1}$$

    This criterion will be derivated in Appendix B.

9. Export all the good points and velocities into a file for further analysis.

A.3 Step III: Statistical studies

Once the file with the sample of points consistent with the initial conditions is produced, one can study the statistical properties of this sample:

- **Statistical distribution of a parameter**: for a given studied parameter, a histogram can be drawn and numerical information such as the median, quartiles or given percentiles can help understand the underlying distribution of this parameter for a given observed velocity kick. Comparing these data for various samples with different initial conditions or observed velocities will help us to establish trends and patterns.

- **Joint distribution of 2 parameters**: for 2 input parameters, a scatter plot on their joint distribution can be drawn. Moreover, we perform Kernel Density Estimation (KDE) methods to construct a joint probability distributions.

- **Range of a parameter**: for a given parameter, we can also just focus on its range, to see if the observed velocity has narrowed it from its original range (or the initial conditions) to a tighter interval.

Construction of the distributions from a sample is complicated by two effects that we take into account:

- The first one is caused by the **uncertainty on the observed velocity**.

  Remember that the observed velocity is an interval (like all initial conditions) but we accept all points with higher total kick than the minimum of the observed velocity (or in the case with β initial condition, with $v_{\parallel}$ and $v_{\perp}$ coherent with any v_r in the interval).

  When the total kick lies close to the lower bound of the observed velocity, we need to reflect that in many cases of velocities in the range, our point would not have made the cut, while if the total kick is higher than the maximum range of the observed velocity, it would make the cut whatever the actual observed velocity may be.

  Therefore we assign each point a weight that will affect in the statistical analysis involving probability distributions. If the total kick lies outside the interval, its weight is 1. Then, we assume that the real observed velocity is distributed uniformly in the given interval. This is, if the interval for observed velocity is $[v_{r1}, v_{r2}]$ then the weight of a point in the parameter space with velocity v_{kick} is:

$$\text{weight} = \begin{cases} 0 & \text{if } v_{\text{kick}} \leq v_{r1} \\ \dfrac{v_{\text{kick}} - v_{r1}}{v_{r2} - v_{r1}} & \text{if } v_{r1} < v_{\text{kick}} < v_{r2} \\ 1 & \text{if } v_{r2} < v_{\text{kick}} \end{cases} \tag{A.2}$$

- The second one is due to the **selection bias produced by the observed velocity measurement**.

  Once we have measured and observed velocity v_r, we need to take into account that orientation of the binary orbit is random with respect to the Earth, as there is no privileged direction. Therefore, being $u(v_{\rm kick})$ a probability density function of velocities for the recoiling BHs in the universe, after a measurement of an observed velocity, the new probability density function is $u'(v_{\rm kick}) = u(v_{\rm kick})/v_{\rm kick}$. This formula is derived in Appendix C.

  A straightforward consequence of that effect is that the statistical distributions for a binary for which we have not measured its radial velocity are not the same that those for a binary for which we measure a radial velocity $v_r = 0$. In the latter case, the binaries with lower kicks will be favored. In a general observation of a radial velocity v_r, total kicks bigger than but closer to v_r are preferred over configurations with much bigger kicks than v_r.

A.4 Example of RALPH use

Let's quickly describe the use of RALPH in a real case. First of all, in the first step we will set a grid on the parameter space simulating an isotropic model. We choose the grid of the following size: $N_q = 19, N_a = 10, N_t = 6, N_p = 6$. Therefore, there is a total of $N = 4,104,000$ cubes. For each cube we compute the minimum and maximum of $\chi_{\rm eff}$ and $\chi_{\rm p}$ over the vertices and the maximum kick and store them in a file.

In Phase II, we use just one initial condition $q = (0.42,\ 0.44)$ and no observed velocity. Note that the case of observing no velocity is also interesting as the output should match the fraction of the parameter space with such initial conditions, so even though the analysis of the intrinsic parameters is useless, analysis of $\chi_{\rm eff}$ and $\chi_{\rm p}$ or total kick can lead to conclusions on the distribution of such parameters.

The analysis of the cubes results in acceptance of a total of $21,600$ cubes. This is a number we already expected, as the only initial condition involves q, and the interval falls exactly inside the partition $[0.40, 0.45]$. Therefore, just 1 in $N_q = 19$ cubes is appropriate for these conditions, giving a total of $4,104,000/19 = 21,600$ cubes.

In the sampling, we specify a size of $N = 10^6$ points. The program runs in a couple of minutes on a laptop computer finding 10^6 points in $2,500,681$ tries. Again,

this is a number we expected, as the only requirement in the sampling is that q, that will be sampled in $[0.40, 0.45]$, falls into the interval $[0.42, 0.44]$. This will happen 40% of the tries, so 2.5 million tries were expected. We now have a number of points with which we can perform statistical studies. The distributions for q, a_1, a_2, θ_1, θ_2 and the total kick v_{kick} of the sample are in figure A.1. We expect flat distributions in q, a_1 and a_2 and sine-like distributions in θ_1 and θ_2.

We can now slightly modify the initial conditions and look at the difference. For example, lets rerun Phase II with the same initial condition $q \in (0.42, 0.44)$ and an observed velocity of $v_r \in [0, 100\ \mathrm{km\,s^{-1}}]$. In this case, the number of selected cubes is the same, $21,600$, and the number of tries to achieve the 10^6 points in the sample has been $2,501,976$, recalling again the 40% efficiency. The distributions have been changed, accordingly to the second effect we described in the Phase III of the algorithm. The distributions for these initial conditions are shown in figure A.2.

We study another modification of the initial conditions and look at the difference. Lets rerun Phase II with the same initial condition $q \in (0.42, 0.44)$ and an observed velocity of $v_r \in [1000, 1100\ \mathrm{km\,s^{-1}}]$. In this case, the number of selected cubes is $13,126$, which indicates that some of the cubes that were selected in the last occasion might have maximum velocities below $1000\ \mathrm{km\,s^{-1}}$ and therefore have been rejected in this case. The number of tries to achieve the 10^6 points in the sample has been $9,629,129$, lasting for about half an hour with a total efficiency of about 10.5%. The distributions for these initial conditions are shown in figure A.3.

Note that in this case, the parameter a_1 has probability 0 for values lower than 0.15. Therefore, by measuring an observed velocity of $v_r = 1050 \pm 50$ km/s in the initial conditions $q = 0.43 \pm 0.01$, we can constrain a_1 to $[0.15, 1]$ or equivalently, to the 85% of its original range.

In the last case we present, we set $v_r \in [2000, 2100\ \mathrm{km\,s^{-1}}]$. The number of selected cubes has decreased to 3984, indicating now that most of the cubes fulfilling the initial conditions are not able to reach kicks as high as the observed velocity. The number of tries to achieve the 10^6 points is $34,665,110$, which corresponds to an intrinsic efficiency of 0.072%. The simulation lasted for one hour and the distributions for such initial conditions are shown in figure A.4.

We observe how the range of a_1 is now a 40% of the original range of the parameter. We also observe that θ_1 range has also been reduced to approximately

55% of its original range. The parameters a_2 and θ_2 still span 100% of the original range. Though a parameter subject to an initial condition may also be studied, it makes no sense to analyze q in this case, as its interval is so narrow that it will be really difficult to find an observed velocity that reduces its range without wiping out completely all the points in the interval.

It is worth noting that increasing kick velocities have the strongest impact on the estimation of the spin magnitude and polar angle of the primary BH, than they do on the corresponding variables of the secondary BH. This confirms the physical intuition that the primary BH is more important at determining the total kick of the binary in general case, while the secondary BH's impact is smaller. By consistently observing these results throughout different experiments we validate that the kick models we are using are consistent with our physical intuition.

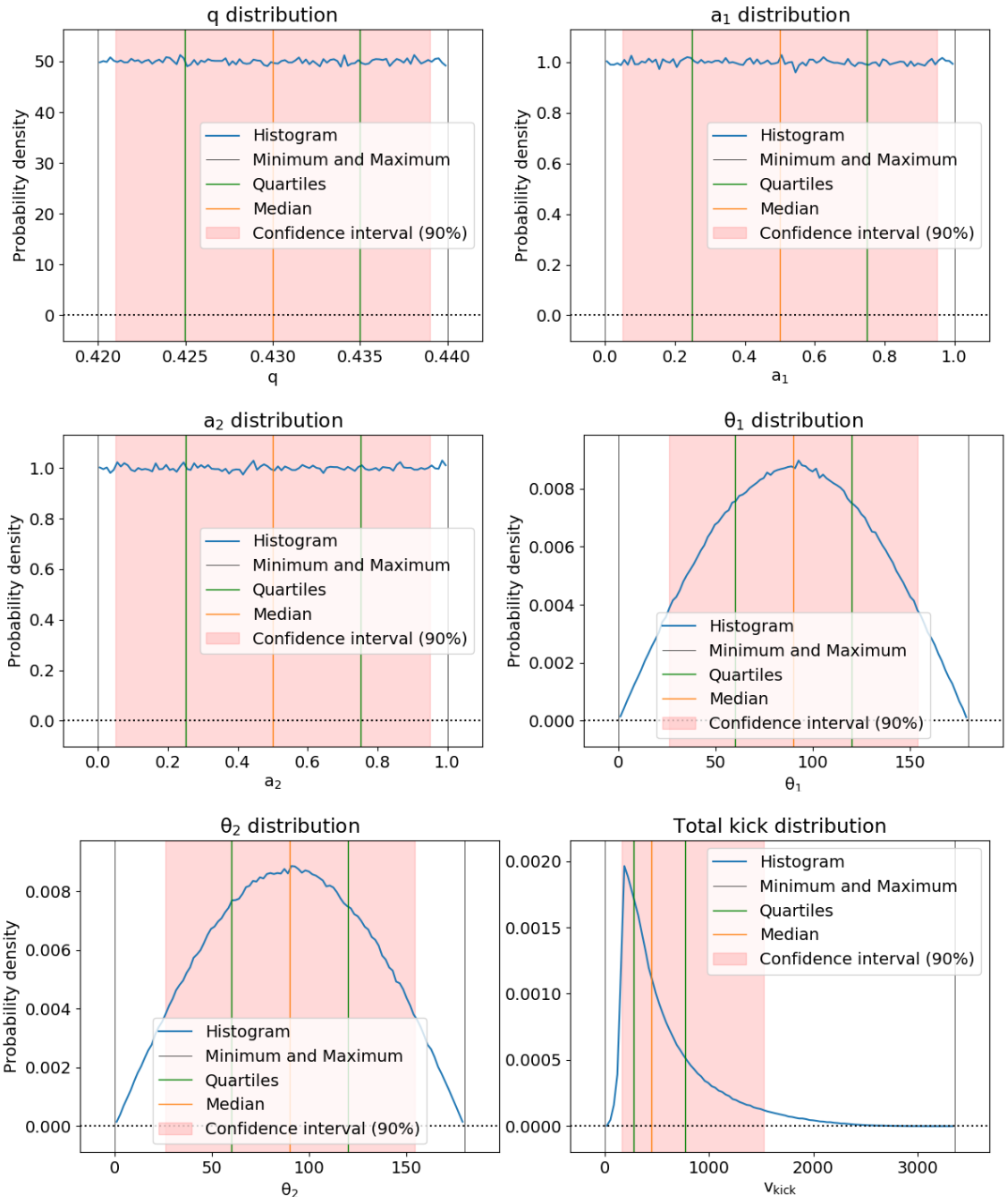

Figure A.1: Probability distributions with the initial condition $q \in [0.42, 0.44]$. We observe flat distributions in q (top left), a_1 (top right) and a_2 (center left), sine-like distributions of θ_1 (center right) and θ_2 (bottom left) and the distribution of the total kick v_{kick} (bottom right).

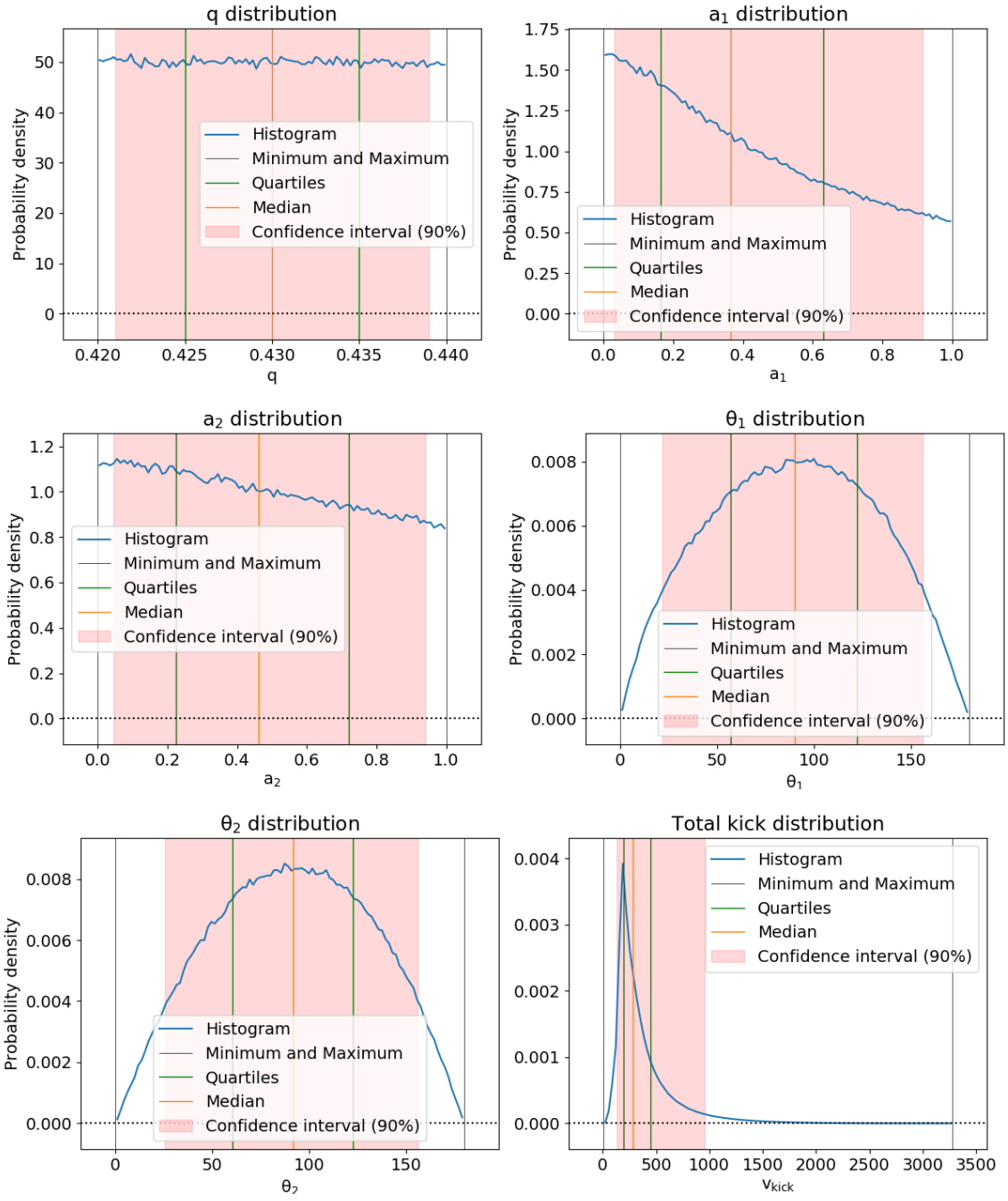

Figure A.2: Probability distributions with the initial conditions $q \in [0.42, 0.44]$ and $v_r \in [0, 100\ \mathrm{km\,s^{-1}}]$

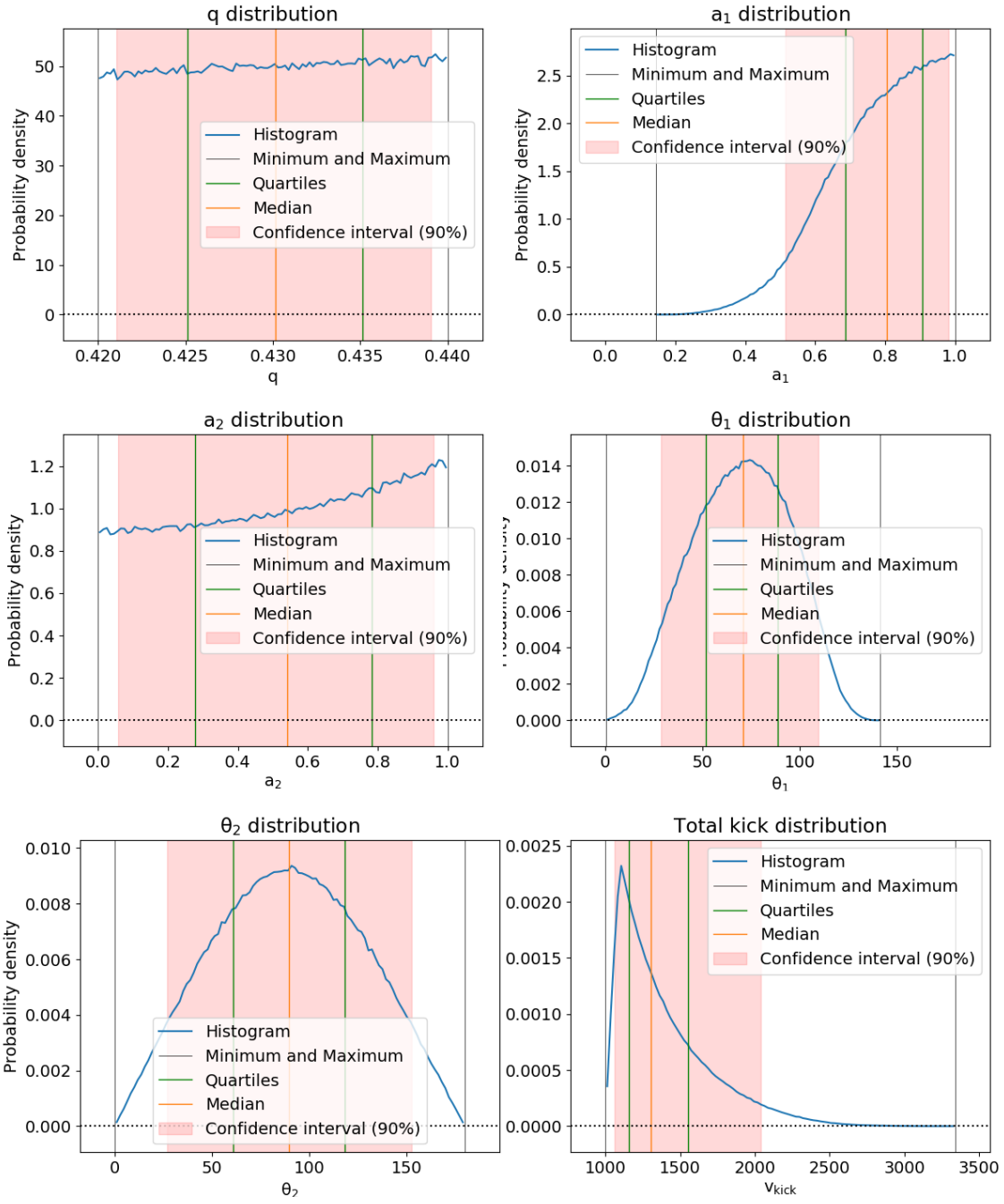

Figure A.3: Probability distributions with the initial conditions $q \in [0.42, 0.44]$ and $v_r \in [1000, 1100\ \mathrm{km\,s^{-1}}]$

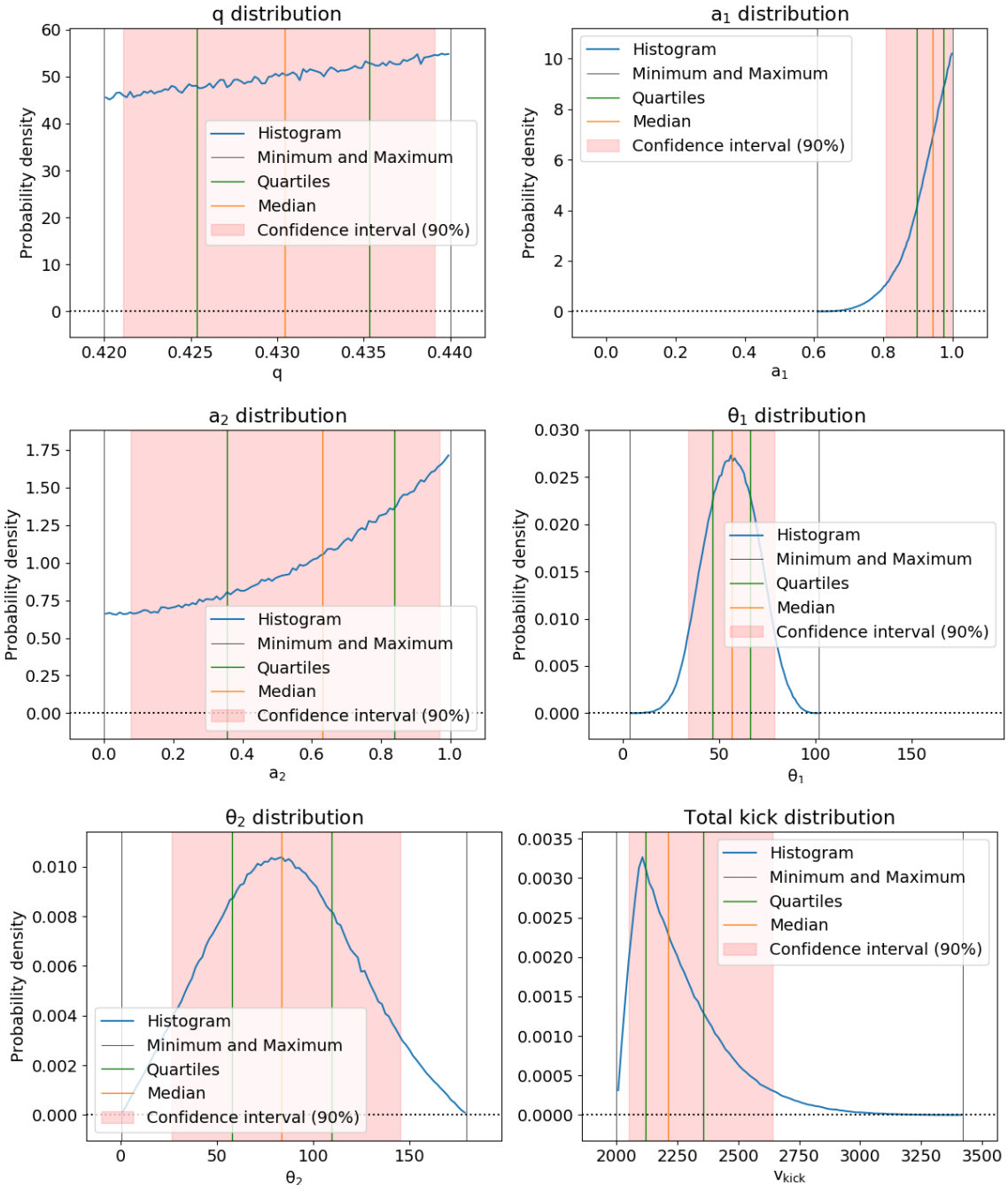

Figure A.4: Probability distributions with the initial conditions $q \in [0.42, 0.44]$ and $v_r \in [2000, 2100\ \mathrm{km\,s^{-1}}]$

Appendix B

Binary inclination

The goal of this appendix is to derive equation (A.1), which is the criterion to accept a point in the parameter space, when we know the binary inclination. Lets first clarify how do we define the inclination of the binary: we will consider the angle β between the orbital angular momentum and the line of sight.

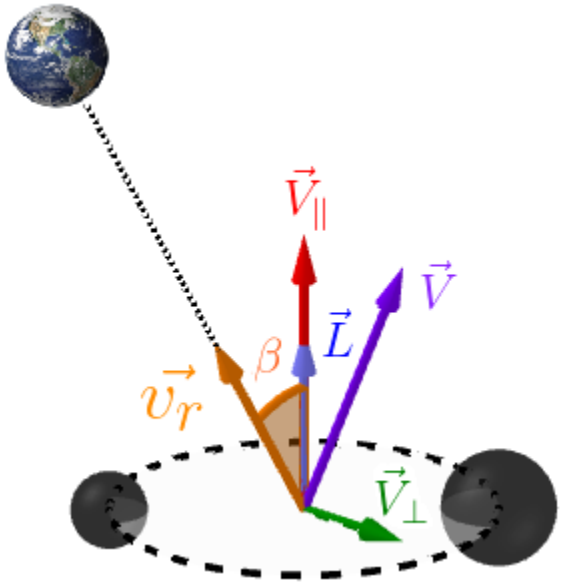

Figure B.1: Geometry of the BBH system and relevant vectors and directions: line of sight (dashed black), orbital angular momentum (blue vector), the parallel component of kick velocity (in red), and the perpendicular component of kick velocity (in green). The purple velocity vector is the sum of the parallel and perpendicular velocities, and $\vec{v_r}$ represents projection of the kick velocity on the line of sight.

Let the origin of coordinates at the point O be the geometric center of the binary orbital plane, and let z-axis be the line of sight. Then, the observer is located at

$E = (0, 0, z), \exists\ z$. We haven't yet fixed the orientation of x and y axis so we will convienently set the binary orbital angular momentum as

$$\hat{\ell} = (\sin\beta\cos\phi,\ \sin\beta\sin\phi,\ \cos\beta)\,,$$

where ϕ the angle between the xz-plane and the plane containing $\hat{\ell}$ and the z-axis. The binary orbital plane is defined as orthogonal to the binary vector, then

$$B : \sin\beta\cos\phi\ x + \sin\beta\sin\phi\ y + \cos\beta\ z = 0.$$

We can define one vector inside the plane by choosing for example $z = 0$, which leads to $\hat{v}_1 = (-\sin\phi, \cos\phi, 0)$ and the orthogonal vector $\hat{v}_2$ fulfilling $\{\hat{v}_1, \hat{v}_2, \hat{\ell}\}$ to be an orthonormal basis: $\hat{v}_2 = \hat{\ell} \times \hat{v}_1 = (-\cos\beta\cos\phi, -\cos\beta\sin\phi, \sin\beta)$. Now let us express $\vec{v_\parallel}$ and $\vec{v_\perp}$ in this base.

$$\vec{v_\parallel} = v_\parallel \hat{\ell} = \left(v_\parallel \sin\beta\cos\phi,\ v_\parallel \sin\beta\sin\phi,\ v_\parallel\cos\beta\right)$$

$$\begin{aligned}\vec{v_\perp} &= v_\perp\left(\cos\delta\ \hat{v}_1 + \sin\delta\ \hat{v}_2\right) = \\ &= (v_\perp\left[-\cos\delta\sin\phi - \cos\beta\sin\delta\cos\phi\right],\qquad v_\perp\left[\cos\delta\cos\phi - \cos\beta\sin\delta\sin\phi\right],\\ &\qquad\qquad\qquad\qquad\qquad\qquad\qquad\qquad\qquad\qquad\qquad\qquad v_\perp\sin\beta\sin\delta)\end{aligned}$$

being δ the angle between $\vec{v_\perp}$ and the vector in the orbital plane $\hat{v}_1$.

Then, $\vec{v}_{\text{kick}} = \vec{v_\parallel} + \vec{v_\perp}$, and we can check that $\vec{v_\parallel}$ and $\vec{v_\perp}$ are indeed perpendicular and $|\vec{v}_{\text{kick}}| = \sqrt{{v_\parallel}^2 + {v_\perp}^2}$. The projection onto the line of sight is a little simpler, as it corresponds to the z component. Then,

$$v_r = v_z = v_\parallel\cos\beta + v_\perp\sin\beta\sin\delta$$

The value of δ is not mesurable since $\hat{v}_1$ is an arbitrary choice. Physically, even though we know the projection angle of the binary, there is a degree of freedom for the direction of $v_\perp$ in the orbital plane. Therefore, we are only able to constrain v_r with:

$$\begin{aligned}v_r &\geq v_\parallel\cos\beta - v_\perp\sin\beta\\ v_r &\leq v_\parallel\cos\beta + v_\perp\sin\beta\end{aligned}$$

which is exactly equation (A.1).

Appendix C

Selection bias in observed velocity measurement

The measurement of an observed kick velocity v_r alters the prior distributions of the parameters of the binaries we might be observing. We shall take into account this to reproduce it accurately in our sample of the parameter space (see page 50). A straightforward effect is that all remnant BHs with $v_{\rm kick}$ lower than the observed radial velocity need to be rejected. In this Appendix we will find that the statistical distributions of the recoiling BHs $u(v_{\rm kick})$ needs to be altered to $u(v_{\rm kick})/v_{\rm kick}$. In the following equations, a normalization constant is assumed to make sure all probability density functions integrate to 1.

The only assumption we are making is that binaries are randomly oriented in the sky, and so are the kicks, since we observe no preferred direction. Then, the angle between the line of sight and the kick is θ and its probability density function is

$$f(\theta)\ \mathrm{d}\theta = \sin\theta\ \mathrm{d}\theta \tag{C.1}$$

Let $v_{\rm kick} = v_0$ be the total velocity of a kick. Then the probability of measuring an observed velocity $v_r = v_0 \cos\theta$ is:

$$\begin{aligned} f(v_r|v_{\rm kick} = v_0)\ \mathrm{d}v_r &= \sin\theta\ \mathrm{d}\theta \qquad (\text{ s.t. } v_r = v_0\cos\theta) \\ &= \frac{\sqrt{{v_0}^2 - {v_r}^2}}{v_0}\ \mathrm{d}v_r\ \left|\frac{\partial\theta}{\partial v_r}\right| \end{aligned} \tag{C.2}$$

Starting from the relationship between the total kick and the observed kick:

$$v_r = v_0 \cos\theta \iff \theta = \arccos\frac{v_r}{v_0} \iff$$
$$\iff \frac{\partial\theta}{\partial v_r} = -\frac{1}{\sqrt{1-\left(\frac{v_r}{v_0}\right)^2}}\ \frac{1}{v_0} = -\frac{1}{\sqrt{{v_0}^2 - {v_r}^2}} \tag{C.3}$$

And therefore, recovering (C.2):

$$f(v_r|v_{\text{kick}} = v_0)\mathrm{d}v_r = \frac{\sqrt{{v_0}^2 - {v_r}^2}}{v_0}\ \mathrm{d}v_r\ \frac{1}{\sqrt{v_0^2 - {v_r}^2}} = \frac{1}{v_0}\ \mathrm{d}v_r \tag{C.4}$$

Let $u(v_{\text{kick}})$ be the kick velocity probability density in our model. Then. the probability of having both a kick v_{kick} and an observed kick v_r is:

$$f(v_{\text{kick}}, v_r)\ \mathrm{d}v_{\text{kick}}\ \mathrm{d}v_r = u(v_{\text{kick}})\ f(v_r; v_{\text{kick}})\ \mathrm{d}v_{\text{kick}}\ \mathrm{d}v_r = \frac{u(v_{\text{kick}})}{v_{\text{kick}}}\ \mathrm{d}v_{\text{kick}}\ \mathrm{d}v_r \tag{C.5}$$

Then, to find the probability of having a kick v_{kick} when observing a kick v_r we need to compute $f(v_{\text{kick}}|v_r)$ and using Bayes' theorem:

$$f(v_{\text{kick}}|v_r)\ \mathrm{d}v_{\text{kick}} \propto f(v_{\text{kick}}, v_r)\ \mathrm{d}v_{\text{kick}} = \frac{u(v_{\text{kick}})}{v_{\text{kick}}}\ \mathrm{d}v_{\text{kick}} \tag{C.6}$$

And this is the result we set out to prove.